Signal Processing 152 (2018) 1–12

Contents lists available at ScienceDirect

Signal Processing

journal homepage: www.elsevier.com/locate/sigpro

Real-valued root-MUSIC for DOA estimation with reduced-dimension EVD/SVD computation

Feng-Gang Yan[a,b], Liu Shuai[a], Jun Wang[a,*], Jun Shi[b,*], Ming Jin[a]

[a] School of information and Electrical Engineering, Harbin Institute of Technology at Weihai, Weihai 264209, China
[b] Communication Research Center, Harbin Institute of Technology, Harbin 150001, China

ARTICLE INFO

Article history:
Received 3 December 2017
Revised 9 May 2018
Accepted 10 May 2018
Available online 22 May 2018

Keywords:
Direction-of-arrival (DOA) estimation
Root multiple signal classification (root-MUSIC)
Reduced-dimension EVD/SVD
Uniform linear array (ULA)
Real-valued computation
Bisymmetric structure

ABSTRACT

A novel real-valued formulation of the popular root multiple signal classification (root-MUSIC) direction of arrival (DOA) estimation technique with substantially reduced computational complexity is developed. The proposed real-valued root-MUSIC (RV-root-MUSIC) algorithm reduces the computational burden mainly in three aspects. First, it exploits the eigenvalue decomposition or the singular value decomposition (EVD/SVD) of a real-valued covariance matrix to extract a real-valued noise subspace, which reduces the complexity by a factor about four as compared to root-MUSIC. Next, based on the bisymmetric or the anti-bisymmetric structure of the real-valued covariance matrix, the real-valued EVD/SVD in RV-root-MUSIC is optimized to be equivalently performed on two sub-matrices with reduced dimensions of about half sizes, which further reduces the complexity by another factor about four as compared to most state-of-the-art real-valued estimators including unitary root-MUSIC (U-root-MUSIC). Finally, the eigenvectors and the singular vectors of those sub-matrices are found of centrosymmetrical or anti-centrosymmetrical structures while the roots of RV-root-MUSIC are proven to appear in conjugate pairs with the form $a + jb$, $a - jb$, which also allows fast coefficient computation and real-valued rooting using Bairstow's method. Numerical simulations illustrate that with significantly reduced complexity, the proposed technique is able to provide good root mean square errors (RMSEs) close to the Cramér–Rao Lower Bound (CRLB).

1. Introduction

In many fields such as radar, sonar, passive localization and wireless communication, there is a need for determining the direction of arrivals (DOAs) of different signals impinging from distinct directions on an array of spatially distributed sensors or antennas [1]. Over several decades, this topic has been extensively studied and numerous algorithms have been proposed. As a majority of traditional spectral search-based methods such as multiple signal classification (MUSIC) [2], maximum-likelihood (ML) [3], subspace fitting [4] and Min-Norm [5] involve high computational complexities, reducing the computational burdens of those estimators has becoming one of the bottleneck techniques in the literature [6–11].

One of the most representative methods for complexity reduction is to exploit some specified array structure to simplify the problem formulation. It is well known that by using the Vandermonde structure of the steering vector of a uniform linear array (ULA), the time consuming spectral search in MUSIC can be equivalently transformed into a simple polynomial rooting step by the popular root-MUSIC algorithm [12]. Taking advantage of the shift invariant array geometry, DOA can be also found with low complexity by the famous estimation of signal parameters via rotational invariance techniques (ESPRIT) [13]. Although root-MUSIC and ESPRIT require no spectral search as compared to MUSIC, conventional versions of those classical algorithms were originally proposed based on complex-valued computations, and consequently, there is a requirement for algorithms demanding more efficient real-valued computations.

Following this idea, a unitary transformation [14] as well as a forward/backward averaging [15,16] technique is proposed to realize real-valued computations. These techniques are investigated for the unitary MUSIC algorithm [17] and extended progressively to a variety of approaches including unitary root MUSIC (U-root-MUSIC) [18], unitary ESPRIT [19], unitary method of direction-of-arrival estimation [20] and unitary matrix pencil [21]. With the special structures of centro-symmetrical arrays (CSAs), those algorithms transform the complex array covariance matrix (ACM) into a real one. It has been proven that this real matrix is symmetri-

* Corresponding author.
E-mail addresses: johnwangstudio@gmail.com (J. Wang), dr.junshi@gmail.com (J. Shi).

https://doi.org/10.1016/j.sigpro.2018.05.009
0165-1684/

cal, and hence, eigenvalue decomposition (EVD) and singular value decomposition (SVD) operations can be implemented with real-valued computations [22]. Since one multiplication between two complex variables require four times that between two real ones, unitary algorithms can reduce the complexity by a factor about four. Besides, it has been found that unitary methods also show improved accuracy as compared to their complex-valued versions [23].

Despite their increased accuracies with reduced costs, almost all of the state-of-the-art unitary transformation-based methods are suitable for only CSAs [24]. To extend real-valued DOA estimation with no dependence on array structures, we have proposed in [25] a real-valued MUSIC (RV-MUSIC) algorithm with arbitrary array geometries. The basic idea is to exploit a real-valued EVD/SVD computation on either the real part of the ACM (R-ACM) or the imaginary part of the ACM (I-ACM) to obtain a real-valued noise subspace. However, it is worth noting that almost all of the existent real-valued methods including RV-MUSIC still involve an EVD/SVD step on an $M\times M$ ACM or on a transformed ACM of the same sizes, where M is the number of sensors. Generally, this EVD/SVD computation requires about $\mathcal{O}(M^3)$ flops [26]. When massive arrays are used [27–29], M can be a very large number and this term of high complexity is still unacceptable.

As a further development of the previous works in [24,25], we propose in this paper a new real-valued root-MUSIC (RV-root-MUSIC) algorithm. We show that under the geometry of a ULA, the R-ACM is a bisymmetric matrix while the I-ACM is an anti-bisymmetric matrix. Based on such a mathematical fact, we provide in-depth analysis in two cases with respect to the parity of M to prove that both the EVD/SVD of the R-ACM and the SVD of the I-ACM can be equivalently computed on two sub-matrices with reduced dimensions of about half sizes. We show that the polynomial coefficients in RV-root-MUSIC are real, and they can be efficiently computed using the centrosymmetrical or anti-centrosymmetrical eigenvectors and singular vectors of those sub-matrices. Thanks to the real coefficients, we show that the roots of RV-root-MUSIC appear in conjugate pairs with the form $a+jb$, $a-jb$, which enable us to exploit Bairstow's method [17,30] for fast rooting with real-valued computations. We finally conduct numerical simulations to verify that with substantially reduced complexity, the proposed approach is able to provide satisfactory performances close to the Cramér–Rao Lower Bound (CRLB) [31].

Notations. Throughout the paper, matrices and vectors are denoted by upper- and lower- boldface letters, respectively. Complex- and real- vectors and matrices are denoted by single-bar- and double-bar- upper boldface letters, respectively, and detailed mathematical notations are defined in Table 1.

Definitions. The following definitions are made in the paper.

1). *Null space*. For an $m\times n$ matrix $\mathbf{A}$, the null space of $\mathbf{A}$ is denoted by null($\mathbf{A}$), given by

$$\text{null}(\mathbf{A}) \triangleq \left\{\boldsymbol{\beta}\in\mathbb{C}^{n\times 1}\middle|\mathbf{A}\boldsymbol{\beta}=\mathbf{0}\right\}. \tag{1}$$

2). Column space. For an $m\times n$ matrix $\mathbf{A}$, the column space of $\mathbf{A}$ is denoted by span($\mathbf{A}$), given by

$$\text{span}(\mathbf{A}) \triangleq \left\{\boldsymbol{\gamma}\in\mathbb{C}^{m\times 1}\middle|\boldsymbol{\gamma}=\sum_{i=1}^{n}k_i\mathbf{a}_i,\ k_i\in\mathbb{C}\right\}. \tag{2}$$

3). *Bisymmetric matrix*. A bisymmetric matrix is a square matrix symmetric about both of its main diagonals, i.e., an $m\times m$ matrix $\mathbf{A}$ is bisymmetric if it satisfies

$$\begin{cases}\mathbf{A}^T=\mathbf{A} & (3.1)\\ \mathbb{J}_m\mathbf{A}\mathbb{J}_m=\mathbf{A}. & (3.2)\end{cases}$$

4). *Anti-bisymmetric matrix*. An anti-bisymmetric matrix is a square matrix which is anti-symmetric about both of its main diagonals, i.e., an $m\times m$ matrix $\mathbf{A}$ is anti-bisymmetric if it satisfies

$$\begin{cases}\mathbf{A}^T=-\mathbf{A} & (4.1)\\ \mathbb{J}_m\mathbf{A}\mathbb{J}_m=-\mathbf{A}. & (4.2)\end{cases}$$

5). *Centrosymmetrical vector*. An $m\times 1$ vector $\mathbf{a}$ is a centrosymmetrical vector if it satisfies

$$\mathbb{J}_m\mathbf{a}=\mathbf{a}. \tag{5}$$

6). *Anti-centrosymmetrical vector*. An $m\times 1$ vector $\mathbf{a}$ is an anti-centrosymmetrical vector if it satisfies

$$\mathbb{J}_m\mathbf{a}=-\mathbf{a}. \tag{6}$$

Table 1
Mathematical notations.

$(\cdot)^T$	Transpose;
$(\cdot)^*$	Conjugation;
$(\cdot)^H$	Hermitian transpose;
$\cap$	Intersection;
$\angle$	Phase angle;
$\lvert\cdot\rvert$	Matrix determinant;
$\lVert\cdot\rVert$	Frobenius norm;
$\mathrm{E}[\cdot]$	Mathematical expectation;
$\mathrm{Re}(\cdot)$	Real part of the embraced element;
$\mathrm{Im}(\cdot)$	Imaginary part of the embraced element;
$\mathbf{0}$	Zero matrix (vector);
$\mathbb{I}_m$	$m\times m$ identity matrix;
$\mathbb{J}_m$	$m\times m$ exchange matrix;
$\mathrm{diag}\{\cdot\}$	Diagonal matrix composed of the embraced elements;
$\mathbf{a}_i$	ith column of matrix $\mathbf{A}$;
$\boldsymbol{\gamma}(i)$	ith element of vector $\boldsymbol{\gamma}$;
$\boldsymbol{\gamma}(i\colon j)$	Sub-vector composed of ith to jth elements of vector $\boldsymbol{\gamma}$.

2. Signal model and literature review

2.1. Signal model

Assume L uncorrelated narrow-band signals $s_l(t)$, $l\in[1,\ L]$ with unknown DOAs $\boldsymbol{\theta}\triangleq\left[\theta_1,\theta_2,\ldots,\theta_L\right]$ simultaneously impinge from far-field on a ULA composed of M antenna elements with inter-sensor spacing d, where L is assumed to be known in advance [2–23]. The inter-sensor spacing d is assumed to satisfy the half-wavelength constraint $d\le\mu/2$, to avoid phase ambiguity caused by the multi-valued property of the sine function, where μ is the wavelength of the narrow-band source. In most subspace-based high-resolution DOA estimators [32], M is generally assumed to be larger than L [2–23]. In the proposed technique, it is assumed $M>2L$, which is reasonable for large ULAs [25,27–29]. Let the first sensor be the reference point, the array output at snapshot t, $t\in[1,\ T]$ can be expressed as

$$\mathbf{x}(t)=\mathbf{A}\mathbf{s}(t)+\mathbf{n}(t), \tag{7}$$

where $\mathbf{A}=\left[\mathbf{a}(\theta_1),\mathbf{a}(\theta_2),\ldots,\mathbf{a}(\theta_L)\right]$ is the $M\times L$ array manifold matrix with each column

$$\mathbf{a}(\theta)=\left[1,e^{j(2\pi/\mu)d\sin\theta},\cdots,e^{j(2\pi/\mu)d(M-1)\sin\theta}\right]^T \tag{8}$$

denoting the $M\times 1$ steering vector, where $j\triangleq\sqrt{-1}$. In addition, $\mathbf{s}(t)$ is the $L\times 1$ signal vector, $\mathbf{n}(t)\sim\mathcal{CN}\left(\mathbf{0},\sigma_n^2\mathbb{I}_M\right)$ is the $M\times 1$ additive noise vector and σ_n^2 is the noise power.

The $M\times M$ forward-only ACM is given by

$$\mathbf{R}=\mathrm{E}\left[\mathbf{x}(t)\mathbf{x}^H(t)\right]=\mathbf{A}\mathbf{R}_s\mathbf{A}^H+\sigma_n^2\mathbb{I}_M, \tag{9}$$

where $\mathbf{R}_s\triangleq\mathrm{E}[\mathbf{s}(t)\mathbf{s}^H(t)]$ is the $L\times L$ signal covariance matrix. As the theoretical ACM is unavailable, we can compute an estimated ACM (EACM) by T snapshots of data as

$$\widehat{\mathbf{R}}=\frac{1}{T}\sum_{t=1}^{T}\mathbf{x}(t)\mathbf{x}^H(t). \tag{10}$$

The EVD/SVDs of the theoretical ACM Eq. (9) and the EACM Eq. (10) can be defined in a standard way as

$$\mathbf{R} = \mathbf{V}\mathbf{\Pi}\mathbf{V}^H = \mathbf{V}_S\mathbf{\Pi}_S\mathbf{V}_S^H + \mathbf{V}_N\mathbf{\Pi}_N\mathbf{V}_N^H \tag{11.1}$$

$$\widehat{\mathbf{R}} = \widehat{\mathbf{V}}\widehat{\mathbf{\Pi}}\widehat{\mathbf{V}}^H = \widehat{\mathbf{V}}_S\widehat{\mathbf{\Pi}}_S\widehat{\mathbf{V}}_S^H + \widehat{\mathbf{V}}_N\widehat{\mathbf{\Pi}}_N\widehat{\mathbf{V}}_N^H, \tag{11.2}$$

respectively, where the subscripts S and N stand for the signal- and noise- subspaces, respectively.

2.2. Literature review

Based on the orthogonality between signal- and the noise- subspaces, the standard MUSIC [3] suggests to search the L minima of the following cost function for source DOAs

$$f_{\text{MUSIC}}(\theta) \triangleq \|\mathbf{a}^H(\theta)\widehat{\mathbf{V}}_N\|^2. \tag{12}$$

Despite its high complexity, standard MUSIC has an easy implementation advantage with arbitrary array geometries [6]. For the special structure of a ULA, the steering vector Eq. (8) can be further written as [12]

$$\mathbf{a}(\theta) = \mathbf{p}(z) \triangleq \left[1, z, z^2, \ldots, z^{M-1}\right]^T, \tag{13}$$

where $z \triangleq e^{j(2\pi/\mu)d\sin\theta}$. The search step in $f_{\text{MUSIC}}(\theta)$ can be replaced by solving the polynomial

$$f_{\text{root-MUSIC}}(z) \triangleq \mathbf{p}^T\left(z^{-1}\right)\widehat{\mathbf{V}}_N\widehat{\mathbf{V}}_N^H\mathbf{p}(z) \tag{14}$$

for the L roots $\widehat{z}_l, l = 1, 2, \ldots, L$ which are located closest to the unit circle, and DOAs are estimated by Rao [12], Pesavento [18], Qian et al. [22]

$$\widehat{\theta}_l = \arcsin\left(\frac{\mu}{2\pi d}\angle\widehat{z}_l\right), \quad l = 1, 2, \ldots, L. \tag{15}$$

Because $\widehat{\mathbf{R}}$ is generally a complex matrix, all the computations in MUSIC and root-MUSIC are complex-valued.

To realize real-valued computation, the U-root-MUSIC algorithm [18] exploits the forward/backward averaging EACM [15,16]

$$\widehat{\mathbf{R}}_{\text{FB}} = \frac{1}{2}\left(\widehat{\mathbf{R}} + \mathbb{J}_M\widehat{\mathbf{R}}^*\mathbb{J}_M\right), \tag{16}$$

with a unitary transformation technique [14–23] to obtain a symmetrical real matrix

$$\widehat{\mathbb{R}} = \text{Re}\left(\mathbf{C}^H\widehat{\mathbf{R}}_{\text{FB}}\mathbf{C}\right), \tag{17}$$

where $\mathbf{C}$ is a complex unitary matrix, given by

$$\mathbf{C} = \frac{1}{\sqrt{2}}\begin{bmatrix}\mathbb{I}_k & j\mathbb{I}_k \\ \mathbb{J}_k & -j\mathbb{J}_k\end{bmatrix}, \ M = 2k \tag{18.1}$$

$$\mathbf{C} = \frac{1}{\sqrt{2}}\begin{bmatrix}\mathbb{I}_k & \mathbf{0} & j\mathbb{I}_k \\ \mathbf{0} & \sqrt{2} & \mathbf{0} \\ \mathbb{J}_k & \mathbf{0} & -j\mathbb{J}_k\end{bmatrix}, \ M = 2k+1. \tag{18.2}$$

By performing real-valued EVD/SVD on $\widehat{\mathbb{R}}$ as

$$\widehat{\mathbb{R}} = \widehat{\mathbb{S}}\widehat{\mathbb{H}}_S\widehat{\mathbb{S}}^H + \widehat{\mathbb{G}}\widehat{\mathbb{H}}_N\widehat{\mathbb{G}}^H, \tag{19}$$

one obtains the U-root-MUSIC polynomial

$$f_{\text{U-root-MUSIC}}(z) \triangleq \tilde{\mathbf{p}}^T\left(z^{-1}\right)\widehat{\mathbb{G}}\widehat{\mathbb{G}}^T\tilde{\mathbf{p}}(z), \tag{20}$$

where $\tilde{\mathbf{p}}(z) \triangleq \mathbf{C}^H\mathbf{p}(z)$. Although $\widehat{\mathbb{G}}$ is real, the coefficients in $f_{\text{U-root-MUSIC}}(z)$ are complex, and hence the polynomial rooting in U-root-MUSIC still involve complex computations.

We have proposed a RV-MUSIC algorithm with arbitrary array geometry in [25]. The key idea of the RV-MUSIC algorithm is shown in Fig. 1, in which

$$\text{span}\left(\mathbb{V}_N\right) \triangleq \text{span}\left(\mathbf{V}_N\right) \cap \text{span}\left(\mathbf{V}_N^*\right)$$

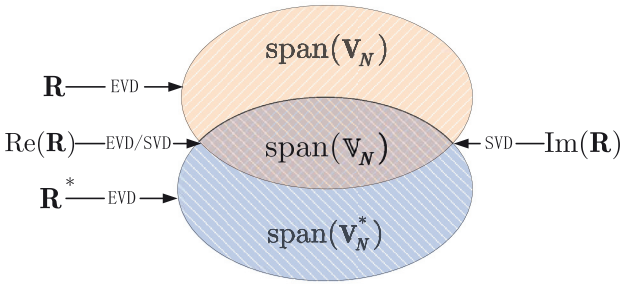

Fig. 1. EVD/SVD on ACM, conjugate ACM, R-ACM and I-ACM.

is a real subspace, denoting the noise intersection [25]. We have shown that the RV-MUSIC spectral

$$f_{\text{RV-MUSIC}}(\theta) \triangleq \|\mathbf{a}^H(\theta)\widehat{\mathbb{V}}_N\|^2 \tag{21}$$

is able to provide similar performance with comparable complexity with unitary MUSIC. In addition, both the EVD/SVD of the R-ACM and the SVD of the I-ACM are performed with only real-valued computations as

$$\text{Re}\left(\mathbf{R}\right) = \mathbb{V}\mathbb{X}\mathbb{V}^T = \mathbb{V}_S\mathbb{X}_S\mathbb{V}_S^T + \mathbb{V}_N\mathbb{X}_N\mathbb{V}_N^T \tag{22.1}$$

$$\text{Im}\left(\mathbf{R}\right) = \mathbb{M}\mathbb{Y}\mathbb{N}^T = \mathbb{M}_S\mathbb{Y}_S\mathbb{N}_S^T + \mathbb{M}_N\mathbb{Y}_N\mathbb{N}_N^T, \tag{22.2}$$

where

$$\mathbb{V}_S = \left[\mathbb{v}_1, \mathbb{v}_2, \ldots, \mathbb{v}_{2L}\right]$$
$$\mathbb{V}_N = \left[\mathbb{v}_{2L+1}, \mathbb{v}_{2L+2}, \ldots, \mathbb{v}_M\right]$$
$$\mathbb{X}_S = \text{diag}\left\{\psi_1, \psi_2, \ldots, \psi_{2L}\right\}$$
$$\mathbb{X}_N = \text{diag}\left\{\psi_{2L+1}, \psi_{2L+2}, \ldots, \psi_M\right\}$$
$$\mathbb{M}_S = \left[\mathbb{m}_1, \mathbb{m}_2, \ldots, \mathbb{m}_{2L}\right]$$
$$\mathbb{M}_N = \left[\mathbb{m}_{2L+1}, \mathbb{m}_{2L+2}, \ldots, \mathbb{m}_M\right]$$
$$\mathbb{N}_S = \left[\mathbb{n}_1, \mathbb{n}_2, \ldots, \mathbb{n}_{2L}\right]$$
$$\mathbb{N}_N = \left[\mathbb{n}_{2L+1}, \mathbb{n}_{2L+2}, \ldots, \mathbb{n}_M\right]$$
$$\mathbb{Y}_S = \text{diag}\left\{\chi_1, \chi_2, \ldots, \chi_{2L}\right\}$$
$$\mathbb{Y}_N = \text{diag}\left\{\chi_{2L+1}, \chi_{2L+2}, \ldots, \chi_M\right\},$$

and ψ and $\mathbb{v}$ stand for the eigenvalue and the eigenvector of Re($\mathbf{R}$), respectively, χ, $\mathbb{m}$ and $\mathbb{n}$ stand for the singular value, the left- and the right- singular vectors of Im($\mathbf{R}$), respectively. It should be noted that there are $2L$ significant eigenvalues and $2L$ significant singular values for Re($\mathbf{R}$) and Im($\mathbf{R}$), respectively [6,25]. It should be also noted that the right singular vectors of Im($\mathbf{R}$) span the same subspace as the noise subspace of Re($\mathbf{R}$) such that [6,25]

$$\text{span}\left(\mathbb{N}_N\right) = \text{span}\left(\mathbb{V}_N\right). \tag{23}$$

Based on the above brief literature review, one can conclude that both conventional complex-valued methods [2–5,12,13] and state-of-the-art real-valued algorithms [14–25] still involve an EVD/SVD computation step on an $M \times M$ matrix, which generally requires about $\mathcal{O}\left(M^3\right)$ flops [26]. When large sensors are used [27–29], M can be a big number, and this term of cost may be computationally very expensive. Therefore, there is a need for DOA estimators demanding less EVD/SVD computations. In the section that follows, we are to show efficient methods for EVD/SVD computations on sub-matrices with reduced dimensions.

3. Reduced-dimension EVD/SVD computation

Because $\mathbf{R}_s$ is diagonal (since the signals are uncorrelated), one can prove that $\mathbf{R}$ is centro-Hermitian such that [14–22]

$$\begin{cases} \mathbb{J}_M\mathbf{R}\mathbb{J}_M = \mathbf{R}^* & (24.1) \\ \mathbb{J}_M\mathbf{R}^*\mathbb{J}_M = \mathbf{R}. & (24.2) \end{cases}$$

Using $\mathrm{Re}(\mathbf{R}) = \frac{1}{2}(\mathbf{R}+\mathbf{R}^*)$ and Eq. (9), we can easily verify $\mathrm{Re}^T(\mathbf{R}) = \mathrm{Re}(\mathbf{R})$. In addition, by using (24), we also obtain

$$\mathbb{J}_M\mathrm{Re}(\mathbf{R})\mathbb{J}_M = \mathrm{Re}(\mathbf{R}). \tag{25}$$

Similarly, by using $\mathrm{Im}(\mathbf{R}) = \frac{1}{2j}(\mathbf{R}-\mathbf{R}^*)$, Eq. (9) and Eq. (24), we can verify $\mathrm{Im}^T(\mathbf{R}) = -\mathrm{Im}(\mathbf{R})$ and

$$\mathbb{J}_M\mathrm{Im}(\mathbf{R})\mathbb{J}_M = -\mathrm{Im}(\mathbf{R}). \tag{26}$$

According to Eq. (3) and Eq. (4), $\mathrm{Re}(\mathbf{R})$ is a bisymmetric matrix while $\mathrm{Im}(\mathbf{R})$ is an anti-bisymmetric matrix. Based on such characteristics, we investigate reduced-dimension computations for the EVD/SVD of $\mathrm{Re}(\mathbf{R})$ and the SVD of $\mathrm{Im}(\mathbf{R})$ with respect to the parity of M in two cases.

3.1. The number of sensors is even such that $M = 2k$

First, let us consider the EVD of $\mathrm{Re}(\mathbf{R})$. With $M = 2k$, we can divide $\mathrm{Re}(\mathbf{R})$ into four $k\times k$ sub-matrices as

$$\mathrm{Re}(\mathbf{R}) = \begin{bmatrix} \mathrm{Re}(\mathbf{R})_{11} & \mathrm{Re}(\mathbf{R})_{12} \\ \mathrm{Re}(\mathbf{R})_{21} & \mathrm{Re}(\mathbf{R})_{22} \end{bmatrix}. \tag{27}$$

Since $\mathrm{Re}^T(\mathbf{R}) = \mathrm{Re}(\mathbf{R})$, we have $\mathrm{Re}(\mathbf{R})_{12} = \mathrm{Re}^T(\mathbf{R})_{21}$. Inserting Eq. (27) into Eq. (25) and using $\mathrm{Re}^T(\mathbf{R}) = \mathrm{Re}(\mathbf{R})$ and $\mathbb{J}_k^2 = \mathbb{I}_k$, it is easy to obtain that

$$\begin{cases} \mathrm{Re}(\mathbf{R})_{22} = \mathbb{J}_k\mathrm{Re}(\mathbf{R})_{11}\mathbb{J}_k & (28-1) \\ \mathbb{J}_k\mathrm{Re}(\mathbf{R})_{21} = \mathrm{Re}^T(\mathbf{R})_{21}\mathbb{J}_k. & (28-2) \end{cases}$$

Using (28-1) and $\mathrm{Re}(\mathbf{R})_{12} = \mathrm{Re}^T(\mathbf{R})_{21}$, Eq. (27) can be simplified with only two $k\times k$ independent sub-matrices $\mathrm{Re}(\mathbf{R})_{11}$ and $\mathrm{Re}(\mathbf{R})_{21}$ as

$$\mathrm{Re}(\mathbf{R}) = \begin{bmatrix} \mathrm{Re}(\mathbf{R})_{11} & \mathrm{Re}^T(\mathbf{R})_{21} \\ \mathrm{Re}(\mathbf{R})_{21} & \mathbb{J}_k\mathrm{Re}(\mathbf{R})_{11}\mathbb{J}_k \end{bmatrix}. \tag{29}$$

By introducing two $k\times k$ sub-matrices $\mathbb{B}_1$ and $\mathbb{B}_2$ as

$$\mathbb{B}_1 \triangleq \mathrm{Re}(\mathbf{R})_{11} - \mathbb{J}_k\mathrm{Re}(\mathbf{R})_{21} \tag{30.1}$$

$$\mathbb{B}_2 \triangleq \mathrm{Re}(\mathbf{R})_{11} + \mathbb{J}_k\mathrm{Re}(\mathbf{R})_{21}, \tag{30.2}$$

we obtain the following theorem, which indicates that in the case $M = 2k$, the EVD/SVD of $\mathrm{Re}(\mathbf{R})$ can be computed by those of $\mathbb{B}_1$ and $\mathbb{B}_2$ equivalently.

Theorem 1. *Let the EVD/SVD of the R-ACM be defined in Eq. (22.1), and let the EVD/SVD of $\mathbb{B}_1$ and that of $\mathbb{B}_2$ be defined in a standard way as*

$$\mathbb{B}_1 = \mathbb{V}_1\mathbb{X}_1\mathbb{V}_1^T = \mathbb{V}_{S,1}\mathbb{X}_{S,1}\mathbb{V}_{S,1}^T + \mathbb{V}_{N,1}\mathbb{X}_{N,1}\mathbb{V}_{N,1}^T \tag{31.1}$$

$$\mathbb{B}_2 = \mathbb{V}_2\mathbb{X}_2\mathbb{V}_2^T = \mathbb{V}_{S,2}\mathbb{X}_{S,2}\mathbb{V}_{S,2}^T + \mathbb{V}_{N,2}\mathbb{X}_{N,2}\mathbb{V}_{N,2}^T. \tag{31.2}$$

With $M = 2k$, the $2k$ eigenvalues of $\mathrm{Re}(\mathbf{R})$ are composed of the k eigenvalues of $\mathbb{B}_1$ and those of $\mathbb{B}_2$ such that

$$\mathbb{X} = \mathrm{diag}\{\mathbb{X}_1, \mathbb{X}_2\}. \tag{32}$$

In addition, the eigenvectors of $\mathrm{Re}(\mathbf{R})$ can be jointed by those of $\mathbb{B}_1$ and $\mathbb{B}_2$ as

$$\begin{cases} \mathbb{V}_S = \begin{bmatrix} \mathbb{V}_{S,1} & \mathbb{V}_{S,2} \\ -\mathbb{J}_k\mathbb{V}_{S,1} & \mathbb{J}_k\mathbb{V}_{S,2} \end{bmatrix} & (33.1) \\ \mathbb{V}_N = \begin{bmatrix} \mathbb{V}_{N,1} & \mathbb{V}_{N,2} \\ -\mathbb{J}_k\mathbb{V}_{N,1} & \mathbb{J}_k\mathbb{V}_{N,2} \end{bmatrix}. & (33.2) \end{cases}$$

Proof. See Appendix A. □

Recalling the definitions Eq. (5) and Eq. (6) as well as observing (33), one can conclude the following corollary for the eigenvectors of $\mathrm{Re}(\mathbf{R})$ immediately.

Corollary 1. *In the case $M = 2k$, the first k eigenvectors of $\mathrm{Re}(\mathbf{R})$ are anti-centrosymmetrical while the last k eigenvectors of $\mathrm{Re}(\mathbf{R})$ are centrosymmetrical.* ■

Next, let us consider the SVD of $\mathrm{Im}(\mathbf{R})$. With $M = 2k$, we can divide $\mathrm{Im}(\mathbf{R})$ into four $k\times k$ sub-matrices as

$$\mathrm{Im}(\mathbf{R}) = \begin{bmatrix} \mathrm{Im}(\mathbf{R})_{11} & \mathrm{Im}(\mathbf{R})_{12} \\ \mathrm{Im}(\mathbf{R})_{21} & \mathrm{Im}(\mathbf{R})_{22} \end{bmatrix}. \tag{34}$$

In a similar way, we insert Eq. (34) into Eq. (26) and use $\mathrm{Im}^T(\mathbf{R}) = -\mathrm{Im}(\mathbf{R})$ as well as $\mathbb{J}_k^2 = \mathbb{I}_k$ to obtain

$$\begin{cases} \mathrm{Im}(\mathbf{R})_{22} = -\mathbb{J}_k\mathrm{Im}(\mathbf{R})_{11}\mathbb{J}_k & (35-1) \\ \mathbb{J}_k\mathrm{Im}(\mathbf{R})_{21} = \mathrm{Im}^T(\mathbf{R})_{21}\mathbb{J}_k. & (35-2) \end{cases}$$

Thus, Eq. (34) is simplified with only two $k\times k$ independent sub-matrices $\mathrm{Im}(\mathbf{R})_{11}$ and $\mathrm{Im}(\mathbf{R})_{21}$ as

$$\mathrm{Im}(\mathbf{R}) = \begin{bmatrix} \mathrm{Im}(\mathbf{R})_{11} & -\mathrm{Im}^T(\mathbf{R})_{21} \\ \mathrm{Im}(\mathbf{R})_{21} & -\mathbb{J}_k\mathrm{Im}(\mathbf{R})_{11}\mathbb{J}_k \end{bmatrix}. \tag{36}$$

By defining two $k\times k$ matrices $\mathbb{D}_1$ and $\mathbb{D}_2$ as

$$\mathbb{D}_1 \triangleq \mathrm{Im}(\mathbf{R})_{11} - \mathbb{J}_k\mathrm{Im}(\mathbf{R})_{21} \tag{37.1}$$

$$\mathbb{D}_2 \triangleq \mathrm{Im}(\mathbf{R})_{11} + \mathbb{J}_k\mathrm{Im}(\mathbf{R})_{21}, \tag{37.2}$$

we obtain the following theorem, which shows that in the case $M = 2k$, the SVD of $\mathrm{Im}(\mathbf{R})$ can be also computed by those of $\mathbb{D}_1$ and $\mathbb{D}_2$ equivalently.

Theorem 2. *Let the SVD of the I-ACM be defined in Eq. (22.2), and let $\mathbb{D}_1$ and $\mathbb{D}_2$ be defined as (37) with their SVDs given by*

$$\mathbb{D}_1 = \mathbb{M}_1\mathbb{Y}_1\mathbb{N}_1^T = \mathbb{M}_{S,1}\mathbb{Y}_{S,1}\mathbb{N}_{S,1}^T + \mathbb{M}_{N,1}\mathbb{Y}_{N,1}\mathbb{N}_{N,1}^T \tag{38.1}$$

$$\mathbb{D}_2 = \mathbb{M}_2\mathbb{Y}_2\mathbb{N}_2^T = \mathbb{M}_{S,2}\mathbb{Y}_{S,2}\mathbb{N}_{S,2}^T + \mathbb{M}_{N,2}\mathbb{Y}_{N,2}\mathbb{N}_{N,2}^T. \tag{38.2}$$

With $M = 2k$, the $2k$ singular values of $\mathrm{Im}(\mathbf{R})$ are composed of the k singular values of $\mathbb{D}_1$ and those of $\mathbb{D}_2$, and we have

$$\mathbb{Y} = \mathrm{diag}\{\mathbb{Y}_1, \mathbb{Y}_2\}. \tag{39}$$

In addition, the eigenvectors of $\mathrm{Im}(\mathbf{R})$ can be jointed by those of $\mathbb{D}_1$ and $\mathbb{D}_2$ as

$$\begin{cases} \mathbb{M}_S = \begin{bmatrix} \mathbb{M}_{S,1} & \mathbb{M}_{S,2} \\ \mathbb{J}_k\mathbb{M}_{S,1} & -\mathbb{J}_k\mathbb{M}_{S,2} \end{bmatrix},\ \mathbb{N}_S = \begin{bmatrix} \mathbb{N}_{S,1} & \mathbb{N}_{S,2} \\ -\mathbb{J}_k\mathbb{N}_{S,1} & \mathbb{J}_k\mathbb{N}_{S,2} \end{bmatrix} & (40.1) \\ \mathbb{M}_N = \begin{bmatrix} \mathbb{M}_{N,1} & \mathbb{M}_{N,2} \\ \mathbb{J}_k\mathbb{M}_{N,1} & -\mathbb{J}_k\mathbb{M}_{N,2} \end{bmatrix},\ \mathbb{N}_N = \begin{bmatrix} \mathbb{N}_{N,1} & \mathbb{N}_{N,2} \\ -\mathbb{J}_k\mathbb{N}_{N,1} & \mathbb{J}_k\mathbb{N}_{N,2} \end{bmatrix}. & (40.2) \end{cases}$$

Proof. See Appendix B. □

One should note that there are L significant singular values for both $\mathbb{D}_1$ and $\mathbb{D}_2$, and these $2L$ singular values compose the $2L$ significant singular values of $\mathrm{Im}(\mathbf{R})$. Also note that the right singular vectors of $\mathrm{Im}(\mathbf{R})$ span the same subspace as the noise subspace of $\mathrm{Re}(\mathbf{R})$, as shown in Eq. (23). Therefore, we observe from (40.2) that the real noise intersection $\mathbb{N}_N$ can be computed by reduced-dimension SVDs on $\mathbb{D}_1$ and $\mathbb{D}_2$. According to the definitions Eq.

(5) and Eq. (6) as well as observing (40), one can conclude the following corollary for the singular vectors of Im(**R**) immediately.

Corollary 2. *In the case $M=2k$, the first k left singular vectors of* Im(**R**) *are centrosymmetrical while the last k left singular vectors of* Im(**R**) *are anti-centrosymmetrical. Oppositely, the first k right singular vectors of* Im(**R**) *are anti-centrosymmetrical while the last k right singular vectors of* Im(**R**) *are centrosymmetrical.* ■

3.2. The number of sensors is odd such that $M=2k+1$.

First, let us investigate the EVD of Re(**R**). Using $\mathrm{Re}^T(\mathbf{R})=\mathrm{Re}(\mathbf{R})$, we can divide Re(**R**) with $M=2k+1$ as

$$\mathrm{Re}(\mathbf{R})=\begin{bmatrix} \underbrace{\mathrm{Re}(\mathbf{R})_{11}}_{k\times k} & \underbrace{\mathbb{d}_1}_{k\times 1} & \underbrace{\mathrm{Re}^T(\mathbf{R})_{21}}_{k\times k} \\ \underbrace{\mathbb{d}_1^T}_{1\times k} & \underbrace{a_1}_{1\times 1} & \underbrace{\mathbb{e}_1^T}_{1\times k} \\ \underbrace{\mathrm{Re}(\mathbf{R})_{21}}_{k\times k} & \underbrace{\mathbb{e}_1}_{k\times 1} & \underbrace{\mathrm{Re}(\mathbf{R})_{22}}_{k\times k} \end{bmatrix}, \tag{41}$$

where a_1 is a scalar. By inserting Eq. (41) into Eq. (25) and using the facts $\mathrm{Re}(\mathbf{R})_{22}=\mathbb{J}_k\mathrm{Re}(\mathbf{R})_{11}\mathbb{J}_k$ and $\mathbb{J}_k\mathrm{Re}(\mathbf{R})_{21}=\mathrm{Re}^T(\mathbf{R})_{21}\mathbb{J}_k$ (as already shown in (28) as well as $\mathbb{e}_1=\mathbb{J}_k\mathbb{d}_1$, we can remove the two dependent elements $\mathrm{Re}(\mathbf{R})_{22}$ and $\mathbb{e}_1$ and simplify Eq. (41) as

$$\mathrm{Re}(\mathbf{R})=\begin{bmatrix} \mathrm{Re}(\mathbf{R})_{11} & \mathbb{d}_1 & \mathrm{Re}^T(\mathbf{R})_{21} \\ \mathbb{d}_1^T & a_1 & \mathbb{d}_1^T\mathbb{J}_k \\ \mathrm{Re}(\mathbf{R})_{21} & \mathbb{J}_k\mathbb{d}_1 & \mathbb{J}_k\mathrm{Re}(\mathbf{R})_{11}\mathbb{J}_k \end{bmatrix}. \tag{42}$$

To simplify the notations, we reuse the definitions for $\mathbb{B}_1$ and $\mathbb{B}_2$ in (30), and further define a $(k+1)\times(k+1)$ matrix

$$\mathbb{B}_3=\begin{bmatrix} a_1 & \sqrt{2}\mathbb{d}_1^T \\ \sqrt{2}\mathbb{d}_1 & \mathbb{B}_2 \end{bmatrix}. \tag{43}$$

The following theorem indicates that in the case of $M=2k+1$, the EVD/SVD of Re(**R**) can be also computed on sub-matrices $\mathbb{B}_1$ and $\mathbb{B}_3$ equivalently.

Theorem 3. *Let* Re(**R**) *be divided as Eq. (42), and let $\mathbb{B}_1$ and $\mathbb{B}_3$ be defined as (30) and Eq. (43), respectively. Let the EVD/SVD of $\mathbb{B}_1$ be defined as Eq. (31.1) and let that of $\mathbb{B}_3$ be defined as*

$$\mathbb{B}_3=\mathbb{V}_3\mathbb{X}_3\mathbb{V}_3^T=\mathbb{V}_{S,3}\mathbb{X}_{S,3}\mathbb{V}_{S,3}^T+\mathbb{V}_{N,3}\mathbb{X}_{N,3}\mathbb{V}_{N,3}^T. \tag{44.1}$$

With $M=2k+1$, the $2k+1$ eigenvalues of Re(**R**) *are composed of the k eigenvalues of $\mathbb{B}_1$ and the $k+1$ eigenvalues of $\mathbb{B}_3$, and we have*

$$\mathbb{X}=\mathrm{diag}\{\mathbb{X}_1,\mathbb{X}_3\}. \tag{45}$$

In addition, the eigenvectors of Re(**R**) *can be jointed by those of $\mathbb{B}_1$ and $\mathbb{B}_3$ as*

$$\begin{cases} \mathbb{V}_S=\begin{bmatrix} \mathbb{V}_{S,1} & \mathbb{V}_{S,3}(2:k+1) \\ \mathbf{0} & \sqrt{2}\mathbb{V}_{S,3}(1) \\ -\mathbb{J}_k\mathbb{V}_{S,1} & \mathbb{J}_k\mathbb{V}_{S,3}(2:k+1) \end{bmatrix} & (46-1) \\ \mathbb{V}_N=\begin{bmatrix} \mathbb{V}_{N,1} & \mathbb{V}_{N,3}(2:k+1) \\ \mathbf{0} & \sqrt{2}\mathbb{V}_{N,3}(1) \\ -\mathbb{J}_k\mathbb{V}_{N,1} & \mathbb{J}_k\mathbb{V}_{N,3}(2:k+1) \end{bmatrix}, & (46-2) \end{cases}$$

where $\mathbb{V}_{N,3}(1)$ and $\mathbb{V}_{S,3}(1)$ are two $1\times(k+1)$ vectors, denoting the first rows of $\mathbb{V}_{N,3}$ and $\mathbb{V}_{S,3}$, respectively, $\mathbb{V}_{N,3}(2:k+1)$ and $\mathbb{V}_{S,3}(2:k+1)$ are two $k\times(k+1)$ matrices composed of the last k rows of $\mathbb{V}_{N,3}$ and $\mathbb{V}_{S,3}$, respectively.

Proof. By defining

$$\mathbb{P}_3\triangleq\frac{1}{\sqrt{2}}\begin{bmatrix} \mathbb{I}_k & \mathbf{0} & \mathbb{I}_k \\ \mathbf{0} & \sqrt{2} & \mathbf{0} \\ -\mathbb{J}_k & \mathbf{0} & \mathbb{J}_k \end{bmatrix} \tag{47.1}$$

$$\mathbb{Q}_2\triangleq\mathrm{diag}\{\mathbb{V}_1,\mathbb{V}_3\} \tag{47.2}$$

$$\mathbb{T}_4\triangleq\mathbb{P}_3\mathbb{Q}_2=\frac{1}{\sqrt{2}}\begin{bmatrix} \mathbb{V}_1 & \mathbb{V}_3(2:k+1) \\ \mathbf{0} & \sqrt{2}\cdot\mathbb{V}_3(1) \\ -\mathbb{J}_k\mathbb{V}_1 & \mathbb{J}_k\mathbb{V}_3(2:k+1) \end{bmatrix}, \tag{47.3}$$

we can find that $\mathbb{T}_4^T\mathrm{Re}(\mathbf{R})\mathbb{T}_4$ is a diagonal matrix, and the remaining proof is similar to Theorem 1. □

It should be noted that $\mathbb{B}_1$ has an EVD/SVD expression form with $M=2k+1$ similar to that with $M=2k$ in Eq. (31.1). In addition, with $M=2k+1$, $\mathbb{B}_1$ has k eigenvalues in total while $\mathbb{B}_3$ has $k+1$. However, the numbers of significant eigenvalues for $\mathbb{B}_1$ and $\mathbb{B}_3$ are the same, both given by L.

Based on the definitions Eq. (5) and Eq. (6), the following corollary holds in the case $M=2k+1$ for the eigenvectors of Re(**R**).

Corollary 3. *In the case $M=2k+1$, the first k eigenvectors of* Re(**R**) *are anti-centrosymmetrical while the last k those are centrosymmetrical. In addition, the center elements of the first k eigenvectors of* Re(**R**) *are zeros.* ■

Finally, let us investigate the SVD of Im(**R**) with $M=2k+1$, in which the following corollary about the singular values of Im(**R**) is needed.

Corollary 4. *In the case $M=2k+1$,* Im(**R**) *must contain at least a zero singular value.*

Proof 1. Using the fact $\mathrm{Im}^T(\mathbf{R})=-\mathrm{Im}(\mathbf{R})$, we have

$$\left|\mathrm{Im}(\mathbf{R})\right|=\left|\mathrm{Im}^T(\mathbf{R})\right|=\left|-\mathrm{Im}(\mathbf{R})\right|=(-1)^{2k+1}\left|\mathrm{Im}(\mathbf{R})\right|=-\left|\mathrm{Im}(\mathbf{R})\right|, \tag{48}$$

which indicates $\left|\mathrm{Im}(\mathbf{R})\right|=0$. Define $\mathbb{F}\triangleq\mathrm{Im}^T(\mathbf{R})\mathrm{Im}(\mathbf{R})$, we have

$$\left|\mathbb{F}\right|=\left|\mathrm{Im}^T(\mathbf{R})\right|\cdot\left|\mathrm{Im}(\mathbf{R})\right|=\left|\mathrm{Im}(\mathbf{R})\right|^2=0. \tag{49}$$

Hence, $\mathbb{F}$ contain at least a zero eigenvalue. As the singular values of Im(**R**) are square roots of the eigenvalues of $\mathbb{F}$ [26], Im(**R**) contain at least a zero singular value accordingly.

Using $\mathrm{Im}^T(\mathbf{R})=-\mathrm{Im}(\mathbf{R})$, we can divide Im(**R**) as

$$\mathrm{Im}(\mathbf{R})=\begin{bmatrix} \underbrace{\mathrm{Im}(\mathbf{R})_{11}}_{k\times k} & \underbrace{-\mathbb{d}_2}_{k\times 1} & \underbrace{-\mathrm{Im}^T(\mathbf{R})_{21}}_{k\times k} \\ \underbrace{\mathbb{d}_2^T}_{1\times k} & \underbrace{a_2}_{1\times 1} & \underbrace{-\mathbb{e}_2^T}_{1\times k} \\ \underbrace{\mathrm{Im}(\mathbf{R})_{21}}_{k\times k} & \underbrace{\mathbb{e}_2}_{k\times 1} & \underbrace{\mathrm{Im}(\mathbf{R})_{22}}_{k\times k} \end{bmatrix}, \tag{50}$$

where a_2 is a scalar. Similarly, by inserting Eq. (50) into Eq. (26) as well as using the facts $\mathrm{Im}^T(\mathbf{R})=-\mathrm{Im}(\mathbf{R})$, $\mathrm{Im}(\mathbf{R})_{22}=-\mathbb{J}_k\mathrm{Im}(\mathbf{R})_{11}\mathbb{J}_k$, $\mathbb{J}_k\mathrm{Im}(\mathbf{R})_{21}=\mathrm{Im}^T(\mathbf{R})_{21}\mathbb{J}_k$ (as already shown in (35) as well as $a_2=0$ and $\mathbb{e}_2=\mathbb{J}_k\mathbb{d}_2$, we can remove the three dependent elements a_2, $\mathbb{e}_2$ and $\mathrm{Im}(\mathbf{R})_{22}$, and simplify Eq. (50) as

$$\mathrm{Im}(\mathbf{R})=\begin{bmatrix} \mathrm{Im}(\mathbf{R})_{11} & -\mathbb{d}_2 & -\mathrm{Im}^T(\mathbf{R})_{21} \\ \mathbb{d}_2^T & 0 & -\mathbb{d}_2^T\mathbb{J}_k \\ \mathrm{Im}(\mathbf{R})_{21} & \mathbb{J}_k\mathbb{d}_2 & -\mathbb{J}_k\mathrm{Im}(\mathbf{R})_{11}\mathbb{J}_k \end{bmatrix}. \tag{51}$$

With $\mathbb{D}_1$ and $\mathbb{D}_2$ be defined in (37), we further define a $(k+1)\times k$ matrix $\mathbb{D}_3$ and a $k\times(k+1)$ matrix $\mathbb{D}_4$ as follows

$$\mathbb{D}_3=\begin{bmatrix} \mathbb{D}_2 \\ \sqrt{2}\mathbb{d}_2^T \end{bmatrix} \tag{52.1}$$

$$\mathbb{D}_4 = \left[-\sqrt{2}\mathbb{d}_2 \quad \mathbb{D}_1\right]. \tag{52.2}$$

We obtain the following theorem indicating that in the case of $M = 2k+1$, the SVD of $\mathrm{Im}(\mathbf{R})$ can be also computed on sub-matrices $\mathbb{D}_3$ and $\mathbb{D}_4$ equivalently.

Theorem 4. *Let* $\mathrm{Im}(\mathbf{R})$ *be divided as Eq. (51) and let* $\mathbb{D}_3$ *and* $\mathbb{D}_4$ *be defined as (52) with their SVDs given by*

$$\mathbb{D}_3 = \mathbb{M}_3\mathbb{Y}_3\mathbb{N}_3^T = \mathbb{M}_{S,3}\mathbb{Y}_{S,3}\mathbb{N}_{S,3}^T + \mathbb{M}_{N,3}\mathbb{Y}_{N,3}\mathbb{N}_{N,3}^T \tag{53.1}$$

$$\mathbb{D}_4 = \mathbb{M}_4\mathbb{Y}_4\mathbb{N}_4^T = \mathbb{M}_{S,4}\mathbb{Y}_{S,4}\mathbb{N}_{S,4}^T + \mathbb{M}_{N,4}\mathbb{Y}_{N,4}\mathbb{N}_{N,4}^T. \tag{53.2}$$

With $M = 2k+1$, *the* $2k+1$ *singular values of* $\mathrm{Im}(\mathbf{R})$ *are composed of the* k *singular values of* $\mathbb{D}_3$, *zero, and the* k *singular values of* $\mathbb{D}_4$ *such that*

$$\mathbb{Y} = \mathrm{diag}\left\{\mathbb{Y}_3, 0, \mathbb{Y}_4\right\}. \tag{54}$$

In addition, the eigenvectors of $\mathrm{Im}(\mathbf{R})$ *can be jointed by those of* $\mathbb{D}_3$ *and* $\mathbb{D}_4$ *as*

$$\begin{cases} \mathbb{M}_S = \begin{bmatrix} \mathbb{M}_{S,3}(2:k+1) & \mathbb{M}_{S,4} \\ \sqrt{2}\mathbb{M}_{S,3}(1) & \mathbf{0} \\ \mathbb{J}_k\mathbb{M}_{S,3}(2:k+1) & -\mathbb{J}_k\mathbb{M}_{S,4} \end{bmatrix}, \\ \mathbb{N}_S = \begin{bmatrix} \mathbb{N}_{S,3} & \mathbb{N}_{S,4}(2:k+1) \\ \mathbf{0} & \sqrt{2}\mathbb{N}_{S,4}(1) \\ -\mathbb{J}_k\mathbb{N}_{S,3} & \mathbb{J}_k\mathbb{N}_{S,4}(2:k+1) \end{bmatrix} \end{cases} \tag{55-1}$$

$$\begin{cases} \mathbb{M}_N = \begin{bmatrix} \mathbb{M}_{N,3}(2:k+1) & \mathbb{M}_{N,4} \\ \sqrt{2}\mathbb{M}_{N,3}(1) & \mathbf{0} \\ \mathbb{J}_k\mathbb{M}_{N,3}(2:k+1) & -\mathbb{J}_k\mathbb{M}_{N,4} \end{bmatrix}, \\ \mathbb{N}_N = \begin{bmatrix} \mathbb{N}_{N,3} & \mathbb{N}_{N,4}(2:k+1) \\ \mathbf{0} & \sqrt{2}\mathbb{N}_{N,4}(1) \\ -\mathbb{J}_k\mathbb{N}_{N,3} & \mathbb{J}_k\mathbb{N}_{N,4}(2:k+1) \end{bmatrix}. \end{cases} \tag{55-2}$$

Proof. Similarly, by defining

$$\mathbb{P}_4 \triangleq \frac{1}{\sqrt{2}}\begin{bmatrix} \mathbb{I}_k & \mathbf{0} & \mathbb{I}_k \\ \mathbf{0} & \sqrt{2} & \mathbf{0} \\ \mathbb{J}_k & \mathbf{0} & -\mathbb{J}_k \end{bmatrix} \tag{56}$$

$$\mathbb{L}_2 \triangleq \mathrm{diag}\{\mathbb{M}_3, \mathbb{M}_4\} \tag{57}$$

$$\mathbb{K}_2 \triangleq \mathrm{diag}\{\mathbb{N}_3, \mathbb{N}_4\} \tag{58}$$

$$\mathbb{T}_5 \triangleq \mathbb{P}_4\mathbb{L}_2 = \frac{1}{\sqrt{2}}\begin{bmatrix} \mathbb{M}_3(2:k+1) & \mathbb{M}_4 \\ \sqrt{2}\cdot\mathbb{M}_3(1) & \mathbf{0} \\ \mathbb{J}_k\mathbb{M}_3(2:k+1) & -\mathbb{J}_k\mathbb{M}_4 \end{bmatrix} \tag{59}$$

$$\mathbb{T}_6 \triangleq \mathbb{P}_3\mathbb{K}_2 = \frac{1}{\sqrt{2}}\begin{bmatrix} \mathbb{N}_3 & \mathbb{N}_4(2:k+1) \\ \mathbf{0} & \sqrt{2}\cdot\mathbb{N}_4(1) \\ -\mathbb{J}_k\mathbb{N}_3 & \mathbb{J}_k\mathbb{N}_4(2:k+1) \end{bmatrix}, \tag{60}$$

we can verify that $\mathbb{T}_5^T\mathrm{Im}(\mathbf{R})\mathbb{T}_6$ is diagonalized, and the remaining proof is similar to Theorem 2. □

Based on theorem 4, the real noise intersection $\mathbb{N}_N$ can be computed by reduced-dimension SVDs on $\mathbb{D}_3$ and $\mathbb{D}_4$ equivalently, which is shown in (55.2). Noting the dimensions of matrices $\mathbb{M}_3$, $\mathbb{N}_3$, $\mathbb{M}_4$ and $\mathbb{N}_4$, we conclude from (55) the following corollary for the singular vectors of $\mathrm{Im}(\mathbf{R})$.

Corollary 5. *In the case* $M = 2k+1$, *the first* $k+1$ *left singular vectors of* $\mathrm{Im}(\mathbf{R})$ *are centrosymmetrical while the last* k *left singular vectors of* $\mathrm{Im}(\mathbf{R})$ *are anti-centrosymmetrical. Oppositely, the first* k *right singular vectors of* $\mathrm{Im}(\mathbf{R})$ *are anti-centrosymmetrical while the last* $k+1$ *right singular vectors are centrosymmetrical.* ■

Until now, we have shown that the EVD/SVD of the theoretical $\mathrm{Re}(\mathbf{R})$ and the SVD of the theoretical $\mathrm{Im}(\mathbf{R})$ can be equivalently computed on sub-matrices with reduced dimensions. In practice, the theoretical $\mathbf{R}$ is unavailable, and we can obtain only $\widehat{\mathbf{R}}$ with T snapshots of observed data according to Eq. (10). Because $T < \infty$, the centro-Hermitian character does not hold for $\widehat{\mathbf{R}}$, and we generally have

$$\begin{cases} \mathbb{J}_M\widehat{\mathbf{R}}\mathbb{J}_M \neq \widehat{\mathbf{R}}^* & (61.1) \\ \mathbb{J}_M\widehat{\mathbf{R}}^*\mathbb{J}_M \neq \widehat{\mathbf{R}}. & (61.2) \end{cases}$$

Consequently, $\mathrm{Re}(\widehat{\mathbf{R}})$ is no longer bisymmetric and $\mathrm{Im}(\widehat{\mathbf{R}})$ is no long anti-bisymmetric such that

$$\begin{cases} \mathbb{J}_M\mathrm{Re}^T(\widehat{\mathbf{R}})\mathbb{J}_M \neq \mathrm{Re}(\widehat{\mathbf{R}}) & (62.1) \\ \mathbb{J}_M\mathrm{Im}^T(\widehat{\mathbf{R}})\mathbb{J}_M \neq -\mathrm{Im}(\widehat{\mathbf{R}}). & (62.2) \end{cases}$$

Fortunately, by using $\mathbb{J}_M^2 = \mathbb{I}_M$, we obtain from Eq. (16) that

$$\begin{cases} \mathbb{J}_M\widehat{\mathbf{R}}_{\mathrm{FB}}\mathbb{J}_M = \frac{1}{2}\left(\mathbb{J}_M\widehat{\mathbf{R}}\mathbb{J}_M + \widehat{\mathbf{R}}^*\right) = \widehat{\mathbf{R}}_{\mathrm{FB}}^* & (63.1) \\ \mathbb{J}_M\widehat{\mathbf{R}}_{\mathrm{FB}}^*\mathbb{J}_M = \frac{1}{2}\left(\mathbb{J}_M\widehat{\mathbf{R}}^*\mathbb{J}_M + \widehat{\mathbf{R}}\right) = \widehat{\mathbf{R}}_{\mathrm{FB}}. & (63.2) \end{cases}$$

Therefore, $\widehat{\mathbf{R}}_{\mathrm{FB}}$ is a centro-Hermitian matrix. In fact, it has been shown in [15] that $\widehat{\mathbf{R}}_{\mathrm{FB}}$ is centro-Hermitian with an arbitrary matrix $\mathbf{R}_s$, and the $\widehat{\mathbf{R}}_{\mathrm{FB}}$ has been used in various algorithms [14–22]. Using (63), one can easily verify

$$\begin{cases} \mathrm{Re}^T(\widehat{\mathbf{R}}_{\mathrm{FB}}) = \mathrm{Re}(\widehat{\mathbf{R}}_{\mathrm{FB}}) & (64.1) \\ \mathbb{J}_M\mathrm{Re}(\widehat{\mathbf{R}}_{\mathrm{FB}})\mathbb{J}_M = \mathrm{Re}(\widehat{\mathbf{R}}_{\mathrm{FB}}), & (64.2) \end{cases}$$

and

$$\begin{cases} \mathrm{Im}^T(\widehat{\mathbf{R}}_{\mathrm{FB}}) = -\mathrm{Im}(\widehat{\mathbf{R}}_{\mathrm{FB}}) & (65.1) \\ \mathbb{J}_M\mathrm{Im}(\widehat{\mathbf{R}}_{\mathrm{FB}})\mathbb{J}_M = -\mathrm{Im}(\widehat{\mathbf{R}}_{\mathrm{FB}}). & (65.2) \end{cases}$$

Therefore, $\mathrm{Re}(\widehat{\mathbf{R}}_{\mathrm{FB}})$ is bisymmetric while $\mathrm{Im}(\widehat{\mathbf{R}}_{\mathrm{FB}})$ is anti-bisymmetric. This enables us to use $\widehat{\mathbf{R}}_{\mathrm{FB}}$ instead of the $\widehat{\mathbf{R}}$ to compute the noise matrix $\widehat{\mathbb{V}}_N$ using the above discussed reduced-dimension EVD/SVD computations in practice.

4. Proposed RV-root-MUSIC algorithm

4.1. Algorithm description

With the real noise intersection matrix $\widehat{\mathbb{V}}_N$ computed with reduced-dimension EVD/SVD computations, we can use the idea of polynomial rooting to obtain the following RV-root-MUSIC cost function

$$f_{\mathrm{RV-root-MUSIC}}(z) \triangleq \mathbf{p}^T\left(z^{-1}\right)\widehat{\mathbb{V}}_N\widehat{\mathbb{V}}_N^T\mathbf{p}(z). \tag{66}$$

Similar to root-MUSIC and U-root-MUSIC, we can find signal DOAs by inserting the roots of $f_{\mathrm{RV-root-MUSIC}}(z)$ that lie closest to the unit circle into Eq. (15). It is worth noting that the roots of $f_{\mathrm{RV-root-MUSIC}}(z)$ have an important property different from those of root-MUSIC and U-root-MUSIC, which is given by the following theorem.

Theorem 5. *The roots of* $f_{\mathrm{RV-root-MUSIC}}(z)$ *appear in both conjugate- and conjugate reciprocal-pairs, that is, if* z_0 *is a root of* $f_{\mathrm{RV-root-MUSIC}}(z)$, *then* z_0^*, $\widetilde{z_0} \triangleq 1/z_0^*$ *and* $\widetilde{z_0^*} = 1/z_0$ *are roots of* $f_{\mathrm{RV-root-MUSIC}}(z)$ *as well.*

Proof. See Appendix C. □

Theorem 5 indicates that the roots of $f_{\mathrm{RV-root-MUSIC}}(z)$ has a different distribution form from those of $f_{\mathrm{root-MUSIC}}(z)$ and $f_{\mathrm{U-root-MUSIC}}(z)$, which is shown in Figs. 2 and 3 for more clear illustrations. In the figures, a ULA composed of $M = 6$ sensors are exploited to estimate $L = 2$ sources at $\theta_1 = 10^\circ$ and $\theta_2 = 30^\circ$, where the signal-to-noise ratio (SNR) is set as SNR = 0 dB and the

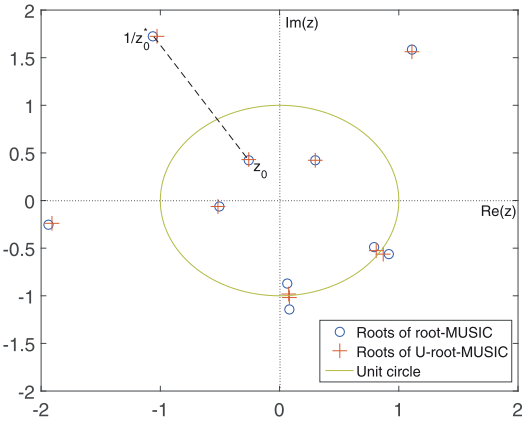

Fig. 2. Roots distribution for root-MUSIC and U-root-MUSIC techniques.

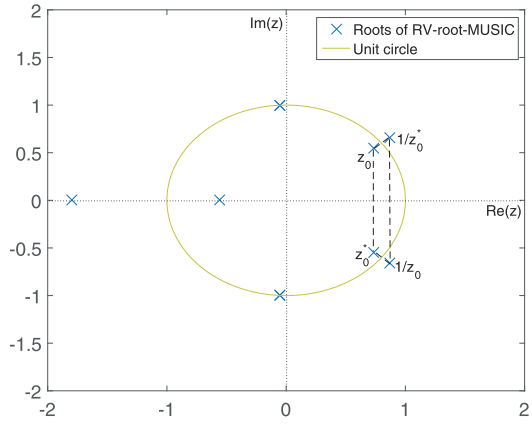

Fig. 3. Roots distribution for the proposed RV-root-MUSIC algorithm.

number of snapshot is set as $T = 100$. As it is seen from Fig. 2 that the roots of $f_{\text{root-MUSIC}}(z)$ and $f_{\text{U-root-MUSIC}}(z)$ appear in only conjugate reciprocity pairs [12,18]. However, it can be concluded from Fig. 3 that the roots of $f_{\text{RV-root-MUSIC}}(z)$ appear in both conjugate- and conjugate reciprocal-pairs.

Suppose that $\theta_l \in \boldsymbol{\theta}$ is one of the signal DOAs, it can be concluded from Theorem 5 that $z_l = e^{j(2\pi/\mu)d\sin\theta_l}$ is one root of $f_{\text{RV-root-MUSIC}}(z)$ that lies closest to the unit circle. In addition, there must be another three corresponding roots z_l^*, $1/z_l$ and $1/z_l^*$ in $f_{\text{RV-root-MUSIC}}(z)$ that also lie closest to the unit circle. Due to the double orthogonality between the noise intersection $\mathbb{V}_N$ and the original steering vector $\mathbf{a}(\theta_l)$ as well as the conjugate steering vector $\mathbf{a}^*(\theta_l) = \mathbf{a}(-\theta_l)$ [25], among the four roots, z_l and $1/z_l^*$ are associated with θ_l while z_l^* and $1/z_l$ are associated with $-\theta_l$. Combining these facts, we can see that for L DOAs $\boldsymbol{\theta}$, there are L roots z_l, $l \in [1, L]$ in $f_{\text{RV-root-MUSIC}}(z)$ that lie closest to the unit circle, which are associated with $\boldsymbol{\theta}$. In addition, there are another L roots $z_l^*, l \in [1, L]$ in $f_{\text{RV-root-MUSIC}}(z)$ that also lie closest to the unit circle, which are associated with $-\boldsymbol{\theta}$. Therefore, we need to select between $\boldsymbol{\theta}$ and $-\boldsymbol{\theta}$ for correct DOA estimation without ambiguity.

Due to its low computational complexity, the conventional beamforming (CBF) [33] is exploited here to solve the ambiguity problem for the proposed technique. Since the steering vector $\mathbf{a}(\theta)$ belongs to the signal subspace at only the true DOAs $\boldsymbol{\theta}$, the CBF spectral amplitudes responding to $\boldsymbol{\theta}$ must be much smaller than those associated with $-\boldsymbol{\theta}$. On the other hand, as the number of the true DOAs, i.e., L, is known in advance, the L true DOAs can be easily selected between $\boldsymbol{\theta}$ and $-\boldsymbol{\theta}$ by

$$\widehat{\boldsymbol{\theta}} = \left\{\widehat{\theta}_1, \widehat{\theta}_2, \cdots, \widehat{\theta}_L\right\} = \arg \min_{\theta \in \left\{\widehat{\boldsymbol{\theta}}, -\widehat{\boldsymbol{\theta}}\right\}} f_{\text{CBF}}(\theta), \tag{67}$$

where the CBF spectral is given by Vasylyshyn [33]

$$f_{\text{CBF}}(\theta) \triangleq \|\mathbf{a}^H(\theta)\widehat{\mathbf{R}}_{\text{FB}}\mathbf{a}(\theta)\|.$$

In summary, the proposed RV-root-MUSIC algorithm structure for DOA estimation with reduced-dimension EVD/SVD computations in cases $M = 2k$ and $M = 2k + 1$ are shown in Figs. 4 and 5, respectively.

Remark 1. Since the proposed method needs to select between $\boldsymbol{\theta}$ and $-\boldsymbol{\theta}$ for the true DOA, the ambiguity may be difficult if two candidate angles lie close to each other. This is because CBF does not provide super-resolution capability, and hence the accuracy of the proposed method may deteriorate in such cases. To solve this problem, we suggest using the standard MUSIC around the estimated angles by the proposed to enhance the accuracy.■

Remark 2. The ULA structure is used to apply the forward/backward averaging technique to make the R-ACM bisymmetric, and this limits the proposed method in some sense. However, there are many techniques such as array interpolation (AI) [34] and beamspace transformation [35] reported to extend array geometries, the new algorithm can be extended to arbitrary array configurations by exploiting these methods. ■

4.2. Complexity reduction

We stress that the proposed method has a significant low-complexity advantage over most state-of-the-art techniques including root-MUSIC and U-root-MUSIC. The reduced complexity is mainly resulted from the following three aspects:

1). The new algorithm exploits real-valued EVD/SVD to calculate the real noise matrix $\widehat{\mathbb{V}}_N$, which obtains a preliminary complexity reduction by a first factor about four as compared to using complex-valued EVD/SVD computations to calculate the complex noise matrix $\widehat{\mathbf{V}}_N$. What's more, the real-valued EVD/SVD computations are optimized to be performed on sub-matrices $\widehat{\mathbb{B}}_1$, $\widehat{\mathbb{B}}_2$, $\widehat{\mathbb{B}}_3$, $\widehat{\mathbb{D}}_1$, $\widehat{\mathbb{D}}_2$, $\widehat{\mathbb{D}}_3$ and $\widehat{\mathbb{D}}_4$, all with reduced dimensions of about half sizes (as shown in (30), (37),(43) and (52)). This provides a further complexity reduction by a second factor about four as compared to state-of-the-art real-valued methods. Combining these facts, the complexity of the subspace decomposition step in RV-root-MUSIC is significantly reduced by a factor about sixteen as compared to root-MUSIC while it is reduced by a factor about four as compared to U-root-MUSIC.

2). Since all the coefficients in $f_{\text{RV-root-MUSIC}}(z)$ are real, the roots of $f_{\text{RV-root-MUSIC}}(z)$ must appear in conjugate pairs with the form $a + jb$, $a - jb$. Consequently, we can exploit Bairstow's method [17,30] to find the roots of $f_{\text{RV-root-MUSIC}}(z)$. This means that the polynomial rooting step in RV-root-MUSIC can be also implemented with real-valued computations. Note that both root-MUSIC and U-root-MUSIC involve complex-valued computations in the polynomial rooting step since the coefficients in both $f_{\text{root-MUSIC}}(z)$ and $f_{\text{U-root-MUSIC}}(z)$ are complex and their roots do not appear in conjugate pairs with the form $a + jb$, $a - jb$. Therefore, the complexity of the polynomial rooting step in RV-root-MUSIC is reduced by a factor about four as compared to both root-MUSIC and U-root-MUSIC.

3). According to Eq. (C.2), the coefficients of z^k in polynomial $f_{\text{RV-root-MUSIC}}(z)$, namely $C_k, k \in [0, M-1]$, can be computed by the product $\widehat{\mathbb{V}}_N\widehat{\mathbb{V}}_N^T$. Because the columns of $\widehat{\mathbb{V}}_N$ are either centrosymmetrical or anti-centrosymmetrical (as shown by corollary 1–corollary 3 and corollary 5), we need to compute only half of

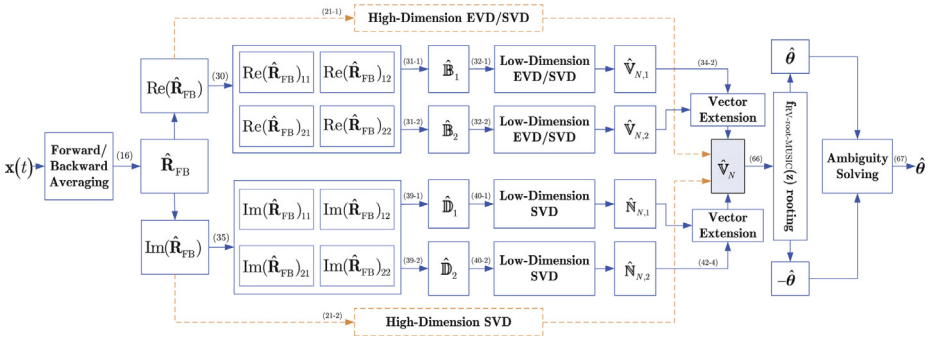

Fig. 4. Algorithm structure of RV-root-MUSIC with $M = 2k$, in which solid lines and boxes are used to describe the proposed algorithm, dashed lines and boxes are provided for comparison, and corresponding equation numbers are given on tops of lines to indicate detailed implementation steps.

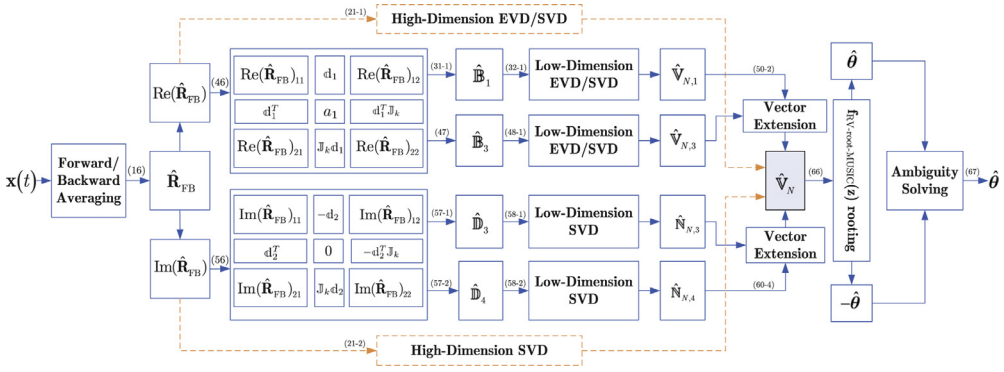

Fig. 5. Algorithm structure of RV-root-MUSIC with $M = 2k + 1$, in which solid lines and boxes are used to describe the proposed algorithm, dashed lines and boxes are provided for comparison, and corresponding equation numbers are given on tops of lines to indicate detailed implementation steps.

Table 2
Complexity comparison among different algorithm in terms of real-valued flops with respect to each implementation step.

Step					
Algorithm	EACM computation	Additional transformation	EVD/SVD	Polynomial coefficient computation	Polynomial rooting
root-MUSIC	$4\times\mathcal{O}(M^2T)$	/	$4\times\mathcal{O}(M^3)$	$4\times\mathcal{O}[M^2(M-L)]$	$4\times\mathcal{O}(M^3)$
U-root-MUSIC	$4\times\mathcal{O}(M^2T)$	/	$\mathcal{O}(M^3)$	$4\times\mathcal{O}[M^2(M-L)]$	$4\times\mathcal{O}(M^3)$
RV-root-MUSIC	$4\times\mathcal{O}(M^2T)$	$4\times\mathcal{O}[(M^2+M)L]$	$1/4\times\mathcal{O}(M^3)$	$1/2\times\mathcal{O}[M^2(M-2L)]$	$\mathcal{O}(M^3)$

the product $\widehat{\mathbb{V}}_N\widehat{\mathbb{V}}_N^T$. On the other hand, to compute the coefficients of z^k, root-MUSIC needs to compute $\widehat{\mathbf{V}}_N\widehat{\mathbf{V}}_N^H$ (as shown in Eq. (14)) while U-root-MUSIC needs to compute $\widehat{\mathbf{C}}^*\widehat{\mathbb{G}}\widehat{\mathbb{G}}^T\widehat{\mathbf{C}}^H$ (as shown in Eq. (20)), both involve complex-valued computations. Therefore, the complexity of the coefficient computation step in RV-root-MUSIC is reduced by a factor about eight as compared to both root-MUSIC and U-root-MUSIC.

Based on the above analysis, we compare the complexity of different algorithms in Table 2, where the complexity is given in terms of real-valued flops with respect to each implementation step. It should be noted that polynomial rooting can be performed by EVD/SVD on a companion matrix by using the Arnoldi iteration method [26,30], which has a same complexity as EVD/SVD. Also note that both the FB Eq. (16) and the unitary transformation Eq. (17) require no additional flops since they involve only element exchange and addition operations. Therefore, the proposed method cost only additional flops for the ambiguity solving problem in Eq. (67), which is given by $4\times\mathcal{O}\big[(M^2+M)L\big]$. It is seen from the table that the proposed technique has a substantially lower complexity as compared the other two methods.

5. Numerical simulations

Numerical simulations with 500 Monte Carlo trials are conducted on a ULA to assess the performance of the proposed estimator and to verify the theoretical analysis. Throughout the simulations, the root mean square error (RMSE) is defined as

$$\text{RMSE} \triangleq 10\log_{10}\sqrt{\frac{1}{500}\sum_{i=1}^{500}\left(\widehat{\theta}_i-\theta\right)^2}, \tag{68}$$

in which $\widehat{\theta}_i$ stands for the ith estimated value for θ. For L sources, the SNR is defined as

$$\text{SNR} \triangleq 10\log_{10}\left[\frac{P_{\text{avg}}}{\sigma_n^2}\right]\ [\text{dB}], \tag{69}$$

where $P_{\text{avg}} = \frac{1}{L}\sum_{l=1}^{L}P_l$ denotes the average power of all sources, and $P_l = E\big[\mathbf{s}_l^2(t)\big]$ is the power of the lth, $l = 1, 2, \cdots, L$ source.

In the first simulation, we verify the correctness of the proposed reduced EVD/SVD computation methods described in

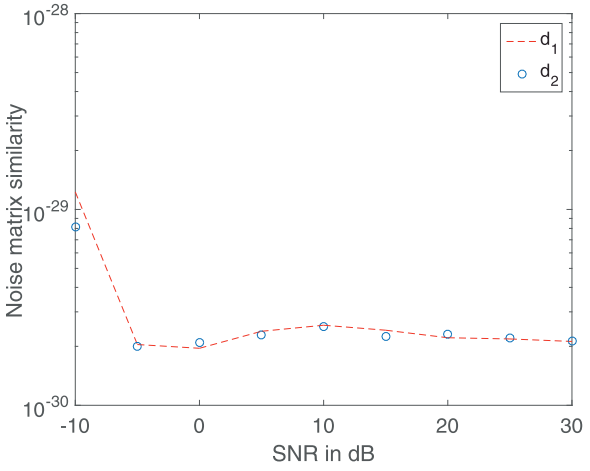

Fig. 6. Noise matrix similarity versus the SNR, $M = 8$ sensors, $L = 2$ signals at $\theta_1 = 30^\circ$ and $\theta_2 = 40^\circ$, $T = 100$ snapshots.

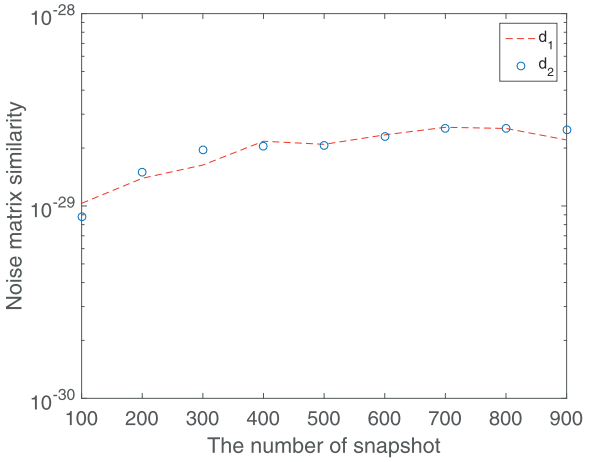

Fig. 7. Noise matrix similarity versus the number of snapshot, $M = 9$ sensors, $L = 2$ signals at $\theta_1 = 30^\circ$ and $\theta_2 = 40^\circ$, SNR = 0 dB.

Section 3. To this end, we define

$$\begin{cases} d_1 \triangleq \left\| \left[\mathbb{I}_M - \widehat{\mathbb{V}}_N(1)\widehat{\mathbb{V}}_N^T(1) \right] \cdot \widehat{\mathbb{V}}_N(2) \right\|^2 & (70-1) \\ d_2 \triangleq \left\| \left[\mathbb{I}_M - \widehat{\mathbb{N}}_N(1)\widehat{\mathbb{N}}_N^T(1) \right] \cdot \widehat{\mathbb{N}}_N(2) \right\|^2, & (70-2) \end{cases}$$

where $\widehat{\mathbb{V}}_N(1)$ and $\widehat{\mathbb{V}}_N(2)$ denote the noise matrices computed by using the high dimension EVD/SVD Eq. (22.1) and the low dimension EVD/SVD given in (33.2) (with $M = 2k$) or (46.2) (with $M = 2k+1$), respectively. $\widehat{\mathbb{N}}_N(1)$ and $\widehat{\mathbb{N}}_N(2)$ denote the noise matrices computed by using the high dimension SVD Eq. (22.2) and the low dimension SVD (40.2) (with $M = 2k$) or (55.2) (with $M = 2k+1$), respectively.

We evaluate d_1 and d_2 with an even M in Fig. 6 and with an odd M in Fig. 7, respectively, where the simulation parameters are given in the figure captions. It is seen clearly from the two figures that

$$d_1 \approx d_2 \approx 0. \quad (71)$$

Because d_1 and d_2 reflect the similarity between the noise matrices computed by using high- and reduced- dimension EVD/SVD methods, we conclude from the two figures that the proposed reduced dimension EVD/SVD computation methods described in Section 3 are correct.

In the second simulation, we compare the proposed RV-root-MUSIC technique with some state-of-the-art popular methods including MUSIC, ESPRIT, root-MUSIC and U-root-MUSIC in terms of RMSE performance. For fair comparison reference, the unconditional CRLB [31] is also applied.

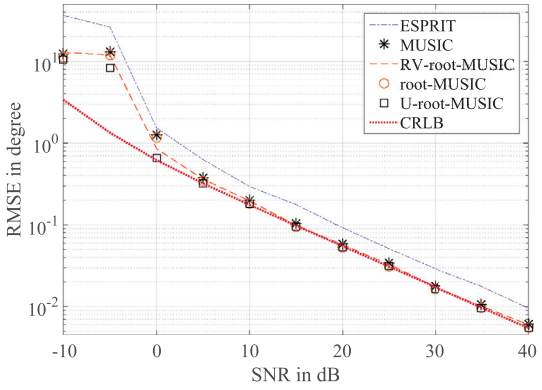

Fig. 8. RMSE versus the SNR with respect to $\theta_1 = 20^\circ$, $M = 10$ sensors, $T = 100$ snapshots, $L = 2$ sources at $\theta_1 = 20^\circ$ and $\theta_2 = 23^\circ$.

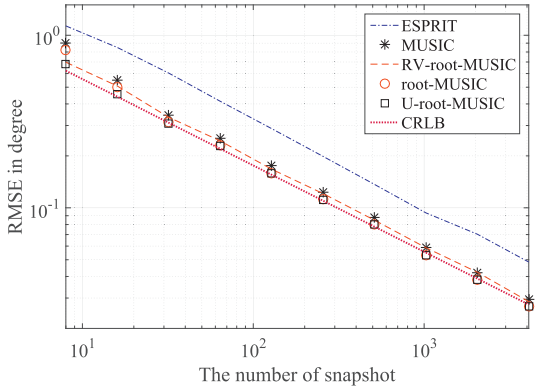

Fig. 9. RMSE versus the number of snapshot with respect to $\theta_2 = 23^\circ$, $M = 10$ sensors, SNR = 10 dB, $L = 2$ sources at $\theta_1 = 20^\circ$ and $\theta_2 = 23^\circ$.

In the first example, we assume $L = 2$ uncorrelated sources at $\theta_1 = 20^\circ$ and $\theta_2 = 23^\circ$, and set the number of sensors as an even number $M = 10$. First, we plot in Fig. 8 the RMSEs of different algorithms as functions of the SNR, where the number of snapshot is fixed as $T = 100$ while the SNR varies over a wide range from SNR $= -10$ dB to SNR $= 40$ dB. Next, we plot in Fig. 9 the RMSEs of different algorithms as functions of the number of snapshots, where the SNR is fixed as SNR $= 10$ dB, and the number of snapshots varies over a wide range from $T = 2^3$ to $T = 2^{12}$.

It can be concluded from Figs. 8 and 9 that the proposed method provides similar performances to MUSIC, and it is much better than ESPRIT. It is also seen from the two figures that root-MUSIC and U-root-MUSIC slightly outperform RV-root-MUSIC at very low SNRs and very small T's (SNR $<$ -0 dB as shown in Fig. 8 and $T < 100$ as shown in Fig. 9). As the SNR and T increase, the RMSEs of RV-root-MUSIC decrease dramatically and the proposed method performs similarly to the other two methods. With mild SNRs and T's (SNR $\geq$ -5 dB as shown in Fig. 8 and $T \geq 100$ as shown in Fig. 9), all of the three polynomial rooting-based estimators and MUSIC provide good RMSEs tend to the CRLB.

In the second example, we assume $L = 3$ uncorrelated sources located at $\theta_1 = 20^\circ$, $\theta_2 = 23^\circ$ and $\theta_3 = 30^\circ$, and set the number of sensors as an odd number $M = 11$ to further compare the performances of the above five algorithms. Similarly to the first example, we plot the RMSEs as functions of the SNRs and those of the number of snapshots in Figs. 10 and 11, respectively. Detailed simulation parameters are given in the captions of Figs. 10 and 11, respectively.

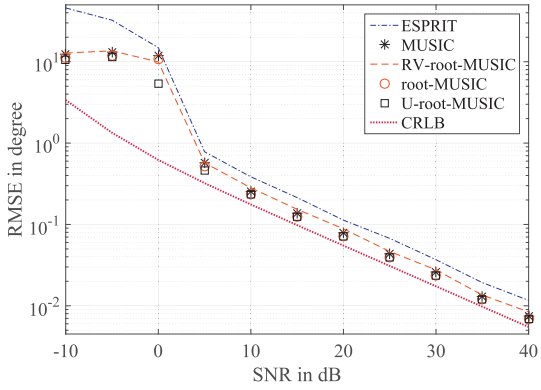

Fig. 10. RMSE versus the SNR with respect to $\theta_1 = 20^\circ$, $M = 11$ sensors, $T = 100$ snapshots, $L = 3$ sources at $\theta_1 = 20^\circ$, $\theta_2 = 23^\circ$ and $\theta_3 = 30^\circ$.

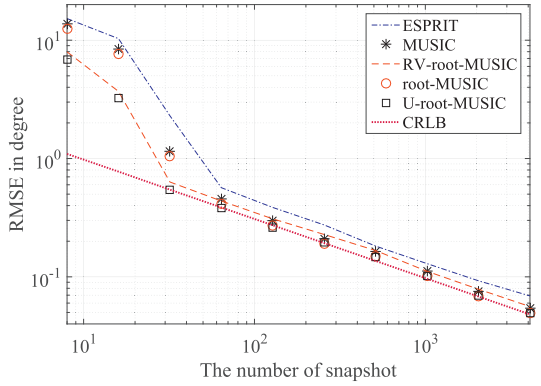

Fig. 11. RMSE versus the number of snapshot with respect to $\theta_2 = 23^\circ$, $M = 11$ sensors, SNR = 10 dB, $L = 3$ sources at $\theta_1 = 20^\circ$, $\theta_2 = 23^\circ$ and $\theta_3 = 30^\circ$.

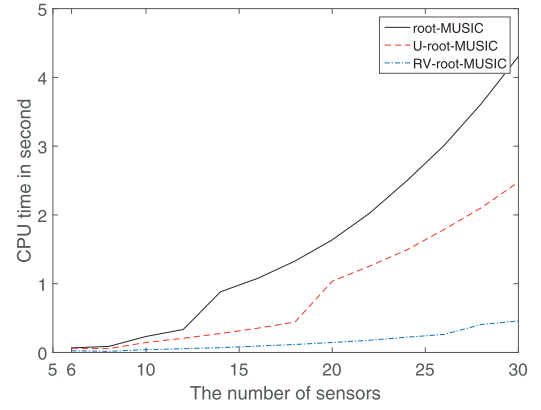

Fig. 12. Simulation time versus the number of sensors, SNR = 0 dB, $T = 100$ snapshots, $L = 2$ sources at $\theta_1 = 20^\circ$ and $\theta_2 = 30^\circ$.

It is seen clearly again from Figs. 10 and 11 that with much better accuracy than ESPRIT, the proposed algorithm shows a similar performance very close to the other three algorithms including MUSIC, root-MUSIC and U-root-MUSIC, all along mild SNRs and T's (SNR ≥ -5dB as shown in Fig. 10 and $T \geq 100$ as shown in Fig. 11). Considering that RV-root-MUSIC only requires a substantially low computational complexity, the new technique makes a sufficiently efficient trade-off between complexity and accuracy.

In the last simulation, we investigate the computational efficiency of the proposed RV-root-MUSIC and compare it with other two polynomial rooting-based methods including root-MUSIC and U-root-MUSIC in Fig. 12. The efficiency is equivalently examined in terms of the CPU times of the three estimators by running the Matlab codes on a PC with Intel(R) Core(TM) Duo T5870 2.0 GHz CPU and 1GB RAM in the same environment. It can be seen from Fig. 12 that RV-root-MUSIC has an obvious efficiency advantage over the other two techniques, and it costs a much lower CPU time than both root-MUSIC and U-root-MUSIC.

6. Conclusions

We have proposed a real-valued version of root-MUSIC for fast DOA estimation, namely, the RV-root-MUSIC algorithm. We have investigated reduced-dimension EVD/SVD computations in detail with respect to the parity of the number of sensors in two cases. We have provided in-depth theoretical analysis to prove that the eigenvalues of the R-ACM and the singular values of the I-ACM are composed of the eigenvalues and the singular values of corresponding sub-matrices divided from the R-ACM and the I-ACM, respectively. Accordingly, the eigenvectors of the R-ACM and the singular vectors of the I-ACM can be equivalently jointed by subvectors decomposed from the corresponding sub-matrices. In addition, we have shown that the real-valued coefficients of the RV-root-MUSIC polynomial can be efficiently computed by the centrosymmetrical or anti-centrosymmetrical vectors of the submatrices. We have further proven that the roots of RV-root-MUSIC appear in conjugate pairs, which allows fast polynomial rooting using Bairstow's method with real-valued computations. As both tasks of EVD/SVD and polynomial rooting are realized with real-valued computations, we conclude that RV-root-MUSIC is much more efficient than root-MUSIC and U-root-MUSIC. Finally, we show by numerical simulations that the proposed approach has a similar performance to root-MUSIC, and hence it makes a substantially efficient trade-off between computational complexity and estimation accuracy.

Acknowledgment

This work is supported by National Natural Science Foundation of China (61501142), Science and Technology Program of WeiHai and Project Supported by Discipline Construction Guiding Foundation in Harbin Institute of Technology (Weihai) (WH20160107).

Appendix A. Proof of Theorem 1

To prove the theorem, we are to diagonalize Re($\mathbf{R}$) with appropriate unitary matrices composed of sub-matrices $\mathbb{B}_1$ and $\mathbb{B}_2$. To this end, we introduce the following $2k \times 2k$ real matrix

$$\mathbb{P}_1 \triangleq \frac{1}{\sqrt{2}}\begin{bmatrix} \mathbb{I}_k & \mathbb{I}_k \\ -\mathbb{J}_k & \mathbb{J}_k \end{bmatrix}. \tag{A.1}$$

It can easily verified that $\mathbb{P}_1^{-1} = \mathbb{P}_1^T$, and therefore, $\mathbb{P}_1$ is a unitary matrix [26]. Using (28.2) and Eq. (29), we have

$$\mathbb{P}_1^T \mathrm{Re}(\mathbf{R})\mathbb{P}_1 = \mathrm{diag}\{\mathbb{B}_1, \mathbb{B}_2\}. \tag{A.2}$$

Notice that $\mathrm{Re}^T(\mathbf{R})_{11} = \mathrm{Re}(\mathbf{R})_{11}$, we obtain by using $\mathbb{J}_k^T = \mathbb{J}_k$ and (28-2) that $\mathbb{B}_1^T = \mathbb{B}_1$ and $\mathbb{B}_2^T = \mathbb{B}_2$. Therefore, both $\mathbb{B}_1$ and $\mathbb{B}_1$ are symmetrical matrices, and their EVD/SVDs require only real-valued computations [26].

Assume that $\{\psi_{1,i}\}_{i=1}^k$ are the k eigenvalues of $\mathbb{B}_1$ with corresponding eigenvectors $\{\mathbb{b}_{1,i}\}_{i=1}^k$, $\{\psi_{2,i}\}_{i=1}^k$ are the k eigenvalues of $\mathbb{B}_2$ with corresponding eigenvectors $\{\mathbb{b}_{2,i}\}_{i=1}^k$, then we have

$$\mathbb{V}_1^T \mathbb{B}_1 \mathbb{V}_1 = \mathrm{diag}\{\psi_{1,1}, \psi_{1,2}, \cdots, \psi_{1,k}\} \tag{A.3.1}$$

$$\mathbb{V}_2^T \mathbb{B}_2 \mathbb{V}_2 = \mathrm{diag}\{\psi_{2,1}, \psi_{2,2}, \cdots, \psi_{2,k}\}. \tag{A.3.2}$$

Using $\mathbb{V}_1$ and $\mathbb{V}_2$ to define a $2k\times 2k$ real matrix

$$\mathbb{Q}_1 \triangleq \begin{bmatrix} \mathbb{V}_1 & \mathbf{0} \\ \mathbf{0} & \mathbb{V}_2 \end{bmatrix} = \mathrm{diag}\{\mathbb{V}_1, \mathbb{V}_2\}, \tag{A.4}$$

with which we further define another $2k\times 2k$ real matrix

$$\mathbb{T}_1 \triangleq \mathbb{P}_1\mathbb{Q}_1 = \frac{1}{\sqrt{2}}\begin{bmatrix} \mathbb{V}_1 & \mathbb{V}_2 \\ -\mathbb{J}_k\mathbb{V}_1 & \mathbb{J}_k\mathbb{V}_2 \end{bmatrix}. \tag{A.5}$$

It is straightforward to obtain

$$\mathbb{T}_1^{-1} = \mathbb{Q}_1^{-1}\mathbb{P}_1^{-1} = \mathbb{Q}_1^T\mathbb{P}_1^T = \mathbb{T}_1^T. \tag{A.6}$$

Thus, $\mathbb{T}_1$ is a unitary matrix [26]. Using Eq. (A.2)–Eq. (A.5), we have

$$\begin{aligned}\mathbb{T}_1^T\mathrm{Re}(\mathbf{R})\mathbb{T}_1 &= \mathbb{Q}_1^T\left[\mathbb{P}_1^T\mathrm{Re}(\mathbf{R})\mathbb{P}_1\right]\mathbb{Q}_1 \\ &= \mathbb{Q}_1^T\mathrm{diag}\{\mathbb{B}_1, \mathbb{B}_2\}\mathbb{Q}_1 \\ &= \mathrm{diag}\left\{\mathbb{V}_1^T\mathbb{B}_1\mathbb{V}_1, \mathbb{V}_2^T\mathbb{B}_2\mathbb{V}_2\right\} \\ &= \mathrm{diag}\{\psi_{1,1}, \cdots, \psi_{1,k}, \psi_{2,1}, \cdots, \psi_{2,k}\},\end{aligned} \tag{A.7}$$

which indicates that $\{\psi_{1,i}\}_{i=1}^k$ and $\{\psi_{2,i}\}_{i=1}^k$ are the $2k$ eigenvalues of $\mathrm{Re}(\mathbf{R})$, and we have Eq. (32).

According to Eq. (A.7), the columns of $\mathbb{T}_1$ are the $2k$ eigenvectors of $\mathrm{Re}(\mathbf{R})$. More specifically, the first k eigenvectors of $\mathrm{Re}(\mathbf{R})$ are associated with $\{\psi_{1,i}\}_{i=1}^k$, which are given by $\mathbb{v}_i = \begin{bmatrix} \mathbb{b}_{1,i} \\ -\mathbb{J}_k\mathbb{b}_{1,i} \end{bmatrix}, i \in [1, k]$, while the last k eigenvectors of $\mathrm{Re}(\mathbf{R})$ are associated with $\{\psi_{2,i}\}_{i=1}^k$, and they are given by $\mathbb{v}_{i+k} = \begin{bmatrix} \mathbb{b}_{2,i} \\ \mathbb{J}_k\mathbb{b}_{2,i} \end{bmatrix}, i \in [1, k]$. Since the coefficient $1/\sqrt{2}$ can be removed without affecting the eigenvectors of $\mathrm{Re}(\mathbf{R})$, and it can be proved that there are L significant eigenvalues for both $\mathbb{B}_1$ and $\mathbb{B}_2$, we obtain (33) immediately. ■

Appendix B. Proof of Theorem 2

Similar to the proof of theorem 1, the primary goal is to choose two unitary matrices for the diagonalization of $\mathrm{Im}(\mathbf{R})$. We introduce the following $2k\times 2k$ real matrix

$$\mathbb{P}_2 \triangleq \frac{1}{\sqrt{2}}\begin{bmatrix} \mathbb{I}_k & \mathbb{I}_k \\ \mathbb{J}_k & -\mathbb{J}_k \end{bmatrix}, \tag{B.1}$$

whose inverse is given by $\mathbb{P}_2^{-1} = \mathbb{P}_2^T$. Hence, $\mathbb{P}_2$ is unitary [26]. Using Eqs. (A.1), (B.1), (36) and $\mathbb{J}_k\mathrm{Im}(\mathbf{R})_{21} = \mathrm{Im}^T(\mathbf{R})_{21}\mathbb{J}_k$, it can be easily verified that

$$\mathbb{P}_2^T\mathrm{Im}(\mathbf{R})\mathbb{P}_1 = \mathrm{diag}\{\mathbb{D}_1, \mathbb{D}_2\}.$$

Let $\{\chi_{1,i}\}_{i=1}^k$ be the k singular values of $\mathbb{D}_1$ and let $\{\chi_{2,i}\}_{i=1}^k$ be the k singular values of $\mathbb{D}_2$, we have

$$\mathbb{M}_1^T\mathbb{D}_1\mathbb{N}_1 = \mathrm{diag}\{\chi_{1,1}, \chi_{1,2}, \cdots, \chi_{1,k}\} \tag{B.2.1}$$

$$\mathbb{M}_2^T\mathbb{D}_2\mathbb{N}_2 = \mathrm{diag}\{\chi_{2,1}, \chi_{2,2}, \cdots, \chi_{2,k}\}. \tag{B.2.2}$$

Using $\mathbb{M}_1$, $\mathbb{M}_2$, $\mathbb{N}_1$ and $\mathbb{N}_2$ to define two $2k\times 2k$ matrices

$$\mathbb{L}_1 \triangleq \mathrm{diag}\{\mathbb{M}_1, \mathbb{M}_2\} \tag{B.3.1}$$

$$\mathbb{K}_1 \triangleq \mathrm{diag}\{\mathbb{N}_1, \mathbb{N}_2\}, \tag{B.3.2}$$

with which we introduce another two $2k\times 2k$ matrices

$$\mathbb{T}_2 \triangleq \mathbb{P}_2\mathbb{L}_1 = \frac{1}{\sqrt{2}}\begin{bmatrix} \mathbb{M}_1 & \mathbb{M}_2 \\ \mathbb{J}_k\mathbb{M}_1 & -\mathbb{J}_k\mathbb{M}_2 \end{bmatrix} \tag{B.4.1}$$

$$\mathbb{T}_3 \triangleq \mathbb{P}_1\mathbb{K}_1 = \frac{1}{\sqrt{2}}\begin{bmatrix} \mathbb{N}_1 & \mathbb{N}_2 \\ -\mathbb{J}_k\mathbb{N}_1 & \mathbb{J}_k\mathbb{N}_2 \end{bmatrix}. \tag{B.4.2}$$

Using (B2.1), (B2) as well as (B.4), we have

$$\begin{aligned}\mathbb{T}_2^T\mathrm{Im}(\mathbf{R})\mathbb{T}_3 &= \mathbb{L}_1^T\left[\mathbb{P}_2^T\mathrm{Im}(\mathbf{R})\mathbb{P}_1\right]\mathbb{K}_1 \\ &= \mathbb{L}_1^T\mathrm{diag}\{\mathbb{D}_1, \mathbb{D}_2\}\mathbb{K}_1 \\ &= \mathrm{diag}\left\{\mathbb{M}_1^T\mathbb{D}_1\mathbb{N}_1, \mathbb{M}_2^T\mathbb{D}_2\mathbb{N}_2\right\} \\ &= \mathrm{diag}\{\chi_{1,1}, \cdots, \chi_{1,k}, \chi_{2,1}, \cdots, \chi_{2,k}\}.\end{aligned} \tag{B.5}$$

which indicates that $\{\chi_{1,i}\}_{i=1}^k$ and $\{\chi_{2,i}\}_{i=1}^k$ are the $2k$ singular values of $\mathrm{Im}(\mathbf{R})$, and we obtain Eq. (39).

In addition, it can be clearly seen from Eq. (B.5) that the columns of $\mathbb{T}_2$ are the $2k$ left singular eigenvectors of $\mathrm{Im}(\mathbf{R})$, the columns of $\mathbb{T}_3$ are the $2k$ right singular eigenvectors of $\mathrm{Im}(\mathbf{R})$. It can be proved that there are L significant singular values for both $\mathbb{D}_1$ and $\mathbb{D}_2$, we obtain (40) by the definitions of $\mathbb{T}_2$ and $\mathbb{T}_3$ in (B.4), which completes the proof. ■

Appendix C. Proof of Theorem 5

Let $C_k, k = -(M-1), \ldots, -1, 0, 1, \ldots, M-1$ be the coefficient of z^k in $\mathbf{p}^T(z^{-1})\widehat{\mathbb{V}}_N\widehat{\mathbb{V}}_N^T\mathbf{p}(z)$, and let $\left(\widehat{\mathbb{V}}_N\widehat{\mathbb{V}}_N^T\right)_{s,t}$ be the sth row and tth column element of $\widehat{\mathbb{V}}_N\widehat{\mathbb{V}}_N^T$, we have

$$\begin{aligned}f_{\mathrm{RV-root-MUSIC}}(z) &= \sum_{k=-(M-1)}^{M-1} C_k z^k = \sum_{s=1}^{M}\sum_{t=1}^{M} z^{-(s-1)}\left(\widehat{\mathbb{V}}_N\widehat{\mathbb{V}}_N^T\right)_{s,t} z^{t-1} \\ &= \sum_{s=1}^{M}\sum_{t=1}^{M}\left(\widehat{\mathbb{V}}_N\widehat{\mathbb{V}}_N^T\right)_{s,t} z^{t-s},\end{aligned} \tag{C.1}$$

which implies that

$$C_k = \sum_{s=1}^{M-k}\left(\widehat{\mathbb{V}}_N\widehat{\mathbb{V}}_N^T\right)_{s,s+k} = \sum_{s=1}^{M-k}\left(\widehat{\mathbb{V}}_N\widehat{\mathbb{V}}_N^T\right)_{s+k,s} = C_{-k}, \quad k \geqslant 0. \tag{C.2}$$

Assume that z_0 is a root of $f_{\mathrm{RV-root-MUSIC}}(z)$, notice that $C_k \in \mathbb{R}, k = -(M-1), \ldots, -1, 0, 1, \ldots, M-1$, we obtain

$$0 = \sum_{k=-(M-1)}^{M-1} C_k z_0^k = \sum_{k=-(M-1)}^{M-1} C_k (z_0^*)^k. \tag{C.3}$$

Therefore, z_0^* is a root of $f_{\mathrm{RV-root-MUSIC}}(z)$. Moreover, it follows directly from Eq. (C.2) and Eq. (C.3) that

$$0 = \sum_{k=-(M-1)}^{M-1} C_k (z_0^*)^k = \sum_{k=-(M-1)}^{M-1} C_{-k} (\widetilde{z}_0)^{-k} = \sum_{k=-(M-1)}^{M-1} C_k (\widetilde{z}_0)^k,$$

which indicates that $\widetilde{z}_0 = 1/z_0^*$ is a root of $f_{\mathrm{RV-root-MUSIC}}(z)$, and consequently, $\widetilde{z}_0^* = 1/z_0$ is also a root of $f_{\mathrm{RV-root-MUSIC}}(z)$. ■

References

[1] J. Krim, M. Viberg, Two decades of array signal processing research: the parametric approach, IEEE Signal Process. Mag. 13 (3) (1996) 67–94.
[2] R.O. Schmidt, Multiple emitter location and signal parameter estimation, IEEE Trans. Antennas Propag. 34 (3) (1986) 276–280.
[3] A.G. Jaffer, Maximum likelihood direction finding of stochastic sources: a separable solution, Proc. ICASSP 5 (1988) 2893–2896.
[4] M. Viberg, B. Ottersten, Sensor array processing based on subspace fitting, IEEE Trans. Signal Process. 39 (5) (1991) 1101–1121.
[5] R. Kumaresan, D.W. Tufts, Estimating the angles of arrival of multiple plane waves, IEEE Trans. Aerosp. Electron. Syst. AES-19 (1) (1983) 134–139.
[6] F.G. Yan, M. Jin, X.L. Qiao, Low-complexity DOA estimation based on compressed MUSIC and its performance analysis, IEEE Trans. Signal Process 61 (8) (2013) 1915–1930.
[7] F.G. Yan, M. Jin, X.L. Qiao, Source localization based on symmetrical MUSIC and its statistical performance analysis, Sci. China Inf. Sci. 56 (6) (2013) 1–13.
[8] F.G. Yan, B. Cao, J.J. Rong, Y. Shen, M. Jin, Spatial aliasing for efficient direction-of-arrival estimation based on steering vector reconstruction, EURASIP J. Adv. Signal Process. (2016) 121.
[9] A. Khabbazibasmenj, et al., Efficient transmit beamspace design for search-free based DOA estimation in MIMO radar, IEEE Trans. Signal Process 62 (6) (2014) 1490–1500.

[10] K. Yu, Low-complexity 2d direction-of-arrival estimation for acoustic sensor arrays, IEEE Signal Process. Letts. 23 (12) (2016) 1791–1795.
[11] V.V. Reddy, M. Mubeen, B.P. Ng, Reduced-complexity super-resolution DOA estimation with unknown number of sources, IEEE Signal Process. Lett. 22 (6) (2015) 772–776.
[12] B.D. Rao, et al., Performance analysis of root-MUSIC, IEEE Trans. Acoust., Speech, Signal Process. 37 (1989) 1939–1949.
[13] R. Roy, T. Kailath, ESPRIT-estimation of signal parameters via rotational invariance techniques, IEEE Trans. Signal Process. 37 (7) (1989) 984–995.
[14] K.C. Huarng, C.C. Yeh, A unitary transformation method for angle-of-arrival estiamtion, IEEE Trans. Signal Process. 39 (1991) 975–977.
[15] D.A. Linebarger, R.D. DeGroat, E.M. Dowling, Efficient direction-finding methods employing forward-backward averaging, IEEE Trans. Signal Process. 42 (8) (1994) 2136–2145.
[16] P. Stoica, M. Jansson, On forward-backward MODE for array signal processing, Digital Signal Process. 7 (4) (1997) 239–252.
[17] J. Selva, Computation of spectral and root MUSIC through real polynomial rooting, IEEE Trans. Signal Process. 53 (5) (2005) 1923–1927.
[18] M. Pesavento, et al., Unitary root-MUSIC with a real-valued eigendecomposition: a theoretical and experimental performance study, IEEE Trans. Signal Process. 48 (5) (2000) 1306–1314.
[19] M. Haardt, F. Romer, Enhancements of unitary ESPRIT for non-circular sources, in: Proc. ICASSP, 2004, pp. 101–104.
[20] A.B. Gershman, P. Stoica, On unitary and forward-backward MODE, Digital Signal Process. 9 (2) (1999) 67–75.
[21] N. Yilmazer, J. Koh, T.K. Sarkar, Utilization of a unitary transform for efficient computation in the matrix pencil method to find the direction of arrival, IEEE Trans. Signal Process. 54 (2006) 175–181.
[22] C. Qian, L. Huang, H.C. So, Improved unitary root-MUSIC for DOA estimation based on pseudo-noise resampling, IEEE Signal Process. Lett 21 (2) (2014) 140–144.
[23] M. Haardt, J.A. Nossek, Unitary ESPRIT: how to obtain increased estimation accuracy with a reduced computational burden, IEEE Trans. Signal Process 43 (5) (1995) 1232–1242.
[24] F.G. Yan, Y. Shen, M. Jin, Fast DOA estimation based on a split subspace decomposition on the array covariance matrix, Signal Processing 115 (2015) 1–8.
[25] F.G. Yan, M. Jin, S. Liu, X.L. Qiao, Real-valued MUSIC for efficient direction estimation with arbitrary array geometries, IEEE Trans. Signal Process. 62 (6) (2014) 1548–1560.
[26] G.H. Golub, C.H.V. Loan, Matrix Computations, The johns Hopkins University Press, Baltimore, MD, 1996.
[27] R. Cao, B. Liu, F. Gao, X. Zhang, A low-complex one-snapshot DOA estimation algorithm with massive ULA, IEEE Communi. Letts. 21 (5) (2017) 1071–1074.
[28] X. Mestre, M.A. Lagunas, Modified subspace algorithms for doa estimation with large arrays, IEEE Trans. Signal Process. 56 (2) (2008) 598–614.
[29] G.T. Pham, P. Loubaton, P. Vallet, Performance analysis of spatial smoothing schemes in the context of large arrays, IEEE Trans. Signal Process. 64 (1) (2016) 160–172.
[30] J. Zhuang, W. Li, A. Manikas, Fast root-MUSIC for arbitrary arrays, Electron. Lett. 46 (2) (2010) 174–176.
[31] P. Stoica, A. Nehorai, Performance study of conditional and unconditional direction-of-arrival estimation, IEEE Trans. Acoust., Speech, Signal Process 38 (9) (1990) 1783–1795.
[32] F.G. Yan, T. Jin, M. Jin, Y. Shen, Subspace-based direction-of-arrival estimation using centro-symmetrical arrays, Eletron. Lett. 27 (11) (2016) 1895–1896.
[33] V. Vasylyshyn, Improving the performance of root-MUSIC via pseudo-noise resampling and conventional beamformer, 2011 Conf. Microwaves, Radar Remote Sensing Symp. (MRRS). 8 (2) (2011) 309–312.
[34] P. Hyberg, M. Jansson, B. Ottersten, Array interpolation and DOA MSE reduction, IEEE Trans. Signal Process., 53 (12) (2005) 4464–4471.
[35] C.P. Mathews, M.D. Zoltowski, Eigenstructure techniques for 2-d angle estimation with uniform circular arrays, IEEE Trans. Signal Process 42 (9) (1994) 2395–2407.